

# Fast Kinetics by Means of Direct and Indirect Electrochemical Techniques

CLAUDE P. ANDRIEUX, PHILIPPE HAPIOT, and JEAN-MICHEL SAVEANT\*

Laboratoire d'Electrochimie Moléculaire de l'Université de Paris 7, Unité Associée au CNRS No. 438, 2 Place Jussieu, 75251 Paris Cedex 05, France

Received January 8, 1990 (Revised Manuscript Received March 22, 1990)

## Contents

I. Introduction	723
II. Direct Methods: Ultramicroelectrodes	725
A. Why Ultramicroelectrodes?	725
B. Instrumentation and Procedures	726
C. Fast Heterogeneous Electron Transfer	728
D. Fast Homogeneous Coupled Reactions	729
III. Indirect Methods: Redox Catalysis	730
A. Indirect vs Direct Methods	730
B. Principle of the Redox Catalysis Method. EC Mechanisms	732
C. Other Mechanisms. Experimental Examples	735
IV. Concluding Remarks	737

## I. Introduction

In the absence of reactant adsorption at the electrode surface, an often fulfilled condition in molecular electrochemistry, the current-limiting phenomena in an electrochemical experiment are of three types: namely, electron transfer at the electrode, coupled homogeneous chemical reactions, and mass transport. In all electrochemical kinetic techniques, information concerning the rate of the two first phenomena is gathered by setting up, in a controlled and reproducible fashion, a competition between them and mass transport.<sup>1,2</sup> In order for the kinetic information of interest to be extracted as safely and simply as possible from the overall current response, mass transport is purposely restricted to diffusion in transient techniques and to diffusion and forced convection in steady-state techniques. The ability of a technique to reach large rate constants of both heterogeneous electron transfer and of coupled homogeneous chemical reactions is thus a function of the possibility to achieve large diffusion rates.

Since the early days of polarography, the ancestor of most electrochemical kinetic techniques, active attention has been paid to determination of the rate constants of coupled homogeneous chemical reactions.<sup>3,4</sup> Since classical polarography does not allow large diffusion rates to be achieved, the method was restricted to CE mechanisms, i.e., electrochemical reactions in which the heterogeneous electron-transfer step is preceded by a homogeneous chemical step

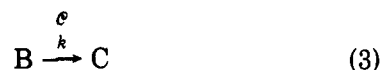


$$K = k_+/k_-$$

$$k = k_+ + k_-$$

and, in this context, to systems in which the A/C equilibrium is much in favor of C. Under such conditions, the limiting current, which is proportional to  $Kk^{1/2}$ , becomes significantly smaller than the diffusion-limiting current, thus allowing the kinetic evaluation of the preceding chemical step. Knowing  $K$  from independent sources, this approach allowed the determination of quite high rate constants in terms of  $k_-$  and was particularly applied to proton-transfer reactions.<sup>5</sup>

Since then, a great number of reactions following a large variety of mechanisms have been kinetically characterized, starting with the EC mechanism in which an irreversible chemical step follows the heterogeneous electron-transfer step

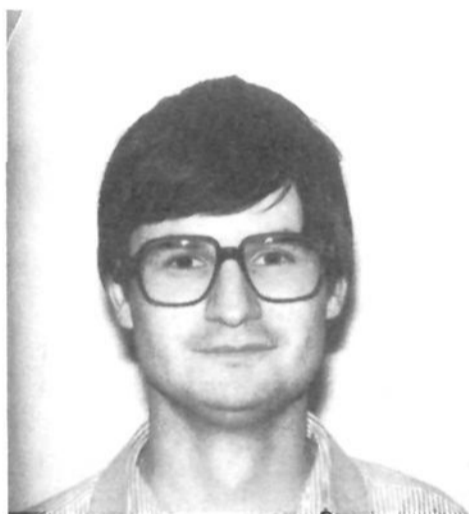


thanks to the development of other electrochemical kinetic techniques allowing much higher diffusion rates to be reached as required from the fact that the C reaction is irreversible. The application of large signal transient techniques such as linear and cyclic voltammetry as well as potential step and double potential step chronoamperometry proved to be particularly fruitful in this connection.<sup>2</sup> Their scope has been considerably extended beyond the simple EC scheme toward bimolecular follow-up reactions and complex sequences of many electron-transfer and coupled homogeneous chemical steps.<sup>2</sup>

In spite of these considerable improvements over classical polarography, two main obstacles have been met when attempting to increase the diffusion rate, i.e., decrease the time window of the technique. One of these derives from the difficulties encountered when attempting to decrease the time constant of the electrochemical cell,  $R_u C_d$ , arising from the charging of the double layer capacitance  $C_d$  through the resistance  $R_u$  between the working and reference electrodes. The other pertains to the distortion of the faradaic responses by the ohmic drop through the  $R_u$  resistance, which rapidly increases as the measurement time is made smaller. As discussed in detail in the next section, these deleterious effects depend upon the size of the working electrode. In the usual applications of electrochemical kinetic techniques, electrodes with a diameter in the millimeter range are currently employed. The surface area of the electrode is then sufficiently small for the technique to be practically nondestructive since the amount of electroactive material that is effectively electrolyzed during each run is negligible. Under these



Claude P. Andrieux was born in Paris, France, in 1942. He received his undergraduate education at the Ecole Supérieure de Physique et Chimie de la Ville de Paris and pursued his graduate studies at the Chemistry Laboratories of the Ecole Normale Supérieure where he received his Docteur-ès-Sciences Physiques degree in 1971. He is presently Directeur de Recherche of the Centre National de la Recherche Scientifique and heads the Laboratoire d'Electrochimie Moléculaire de l'Université de Paris 7. His current research interests include mechanisms and reactivity in organic electrochemistry, fast electrochemical techniques, and conducting organic polymers.



Philippe Hapiot was born in Paris, France, in 1960 and obtained his Ph.D. from the University of Paris 7 in 1988. His present position is Chargé de Recherche of the Centre National de la Recherche Scientifique. He is now spending a postdoctoral stay in the National Institute of Standards and Technology. His current research interests include the investigation of fast electron transfer, proton transfer, and cleavage reactions by means of ultramicroelectrode techniques, pulse radiolysis, and laser flash photolysis.

conditions, intermediates having, at the shortest, lifetimes of fractions of a millisecond can be detected and their decay kinetics quantitatively determined.

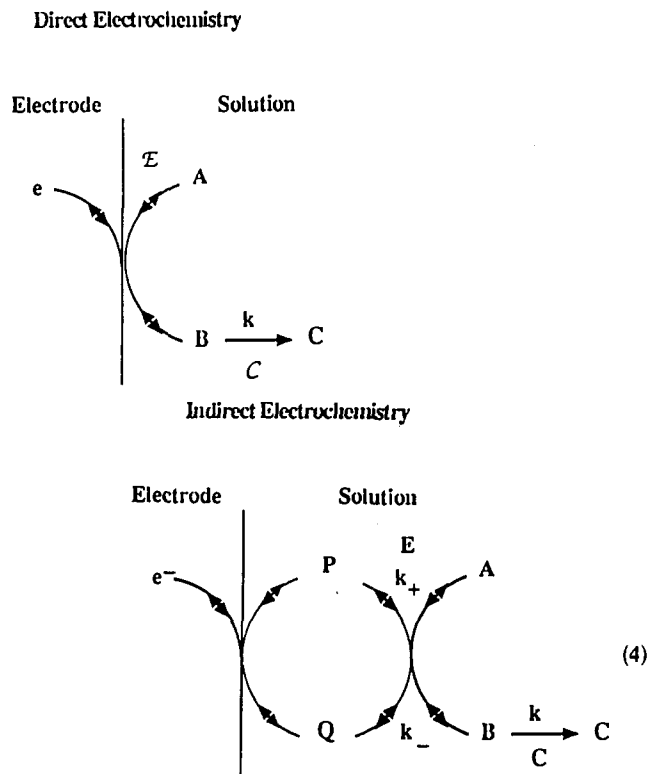
During the last 5 years, more successful attempts have been made to overcome these limitations thanks to the use of working electrodes having a diameter in the micrometer range. Since the millimetric electrodes conventionally used in electrochemical kinetic techniques are already microelectrodes, as compared to electrodes for preparative-scale electrolyses, we will term the micrometric electrodes ultramicroelectrodes according to a usage already well installed. Since it represents the most significant recent advance in the application of direct electrochemical techniques to fast kinetics, the description of their use in the detection and quantitative kinetic characterization of short-lived intermediates is the object of the first part of this review. It will be seen that an improvement of ca. 2 orders of magnitude has been reached in the present



Jean-Michel Savéant was born in Brittany, France, in 1933. He received his undergraduate education at Ecole Normale Supérieure and completed his graduate studies in the Chemistry Laboratories of the same school. He received his Docteur-ès-Sciences Physiques degree in 1966. He was then the Vice-Director of the Laboratoire de Chimie de l'Ecole Normale Supérieure until 1971 when he moved with his research group to the University of Paris 7. He was a Professor there until 1985 when he became Directeur de Recherche au Centre National de la Recherche Scientifique. His research interests are centered on mechanisms and reactivity in molecular electrochemistry with particular recent emphasis on catalysis, modified electrodes, electrochemical engineering, ultramicroelectrodes, and applications to electron-transfer chemistry of organic and organometallic systems and of bioinorganic model molecules.

state of the art, pushing the limit down to the submicrosecond range. We will discuss the application of ultramicroelectrode techniques not only to the kinetic characterization of coupled homogeneous reactions but also the kinetics of the heterogeneous electron transfer itself. The limitations encountered in the determination of the rate constants of fast electron-transfer steps are indeed of the same type as for the coupled homogeneous step since they are likewise caused by limits in the ability to achieve high diffusion rates.

Before the ultramicroelectrode techniques started to be employed, indirect methods were developed in an effort to overcome the above-described limitations borne by the direct techniques. The most successful indirect method in this respect has been the redox catalysis method, whose development commenced in the late 1970s. The basic idea of the method is that the electrode reduction (or oxidation) of substrate A is replaced by its reduction (or oxidation) by a mediator Q generated from the reduction (or oxidation) of its oxidized (reduced) form P at the electrode surface as illustrated with the simple case of an EC mechanism. The mediator is such as to belong to a reversible couple in both the electrochemical and chemical sense and to be easier to reduce (or to oxidize) than the substrate. Much larger rate constants for the decay of short-lived intermediates, such as B, can be measured in this way, the lifetime limit being pushed down to the nanosecond range. As in direct electrochemical techniques, far more complex reaction schemes than the EC mechanism can be investigated. On the other hand, the method is not suited to intermediates having lifetimes above 10  $\mu$ s. Thus, before the ultramicroelectrode techniques appeared, there was a gap (in the region 100–10  $\mu$ s) between the lifetime accessible by direct and indirect electrochemical techniques, respectively. Not only is the gap now filled, but the consistency of the data ob-



tained by the two techniques can be tested in the region where their capabilities overlap. In addition, the method allows one to obtain valuable kinetic and thermodynamic information concerning the homogeneous electron transfer,  $Q + A \leftrightarrow P + B$ , that triggers the overall process. After a brief description of other indirect electrochemical techniques, the possibilities offered by the redox catalysis approach in the kinetic investigation of homogeneous electron transfer as well as associated chemical steps will be described in the second part of this review.

The quantitative kinetic analyses that these various methods permit are obviously of key importance in development of molecular electrochemistry in terms of mechanisms and reactivity, which, besides its own fundamental interest, forms a rational basis for synthetic strategies in preparative-scale electrolysis. They are also important since they quite often deal with homogeneous reactions coupled with electron transfer in the comprehension of many problems of electron-transfer chemistry in general.<sup>6-8</sup>

## II. Direct Methods: Ultramicroelectrodes

### A. Why Ultramicroelectrodes?

Figure 1A shows the cyclic voltammogram of a chemically reversible couple, anthracene/anthracene anion radical, as a function of the scan rate. The current contains two contributions, the faradaic current, which shows a reversible behavior as the scan is reversed, and the double-layer charging current, which rises from zero to an approximately constant value at the foot of the faradaic wave. The phenomena responsible for this typical pattern are summarized in Figure 1B under the form of an equivalent electrical circuit of the electrochemical cell for the three-electrode configuration employed in the experiment. The rising portion of the double-layer charging current is governed by the re-

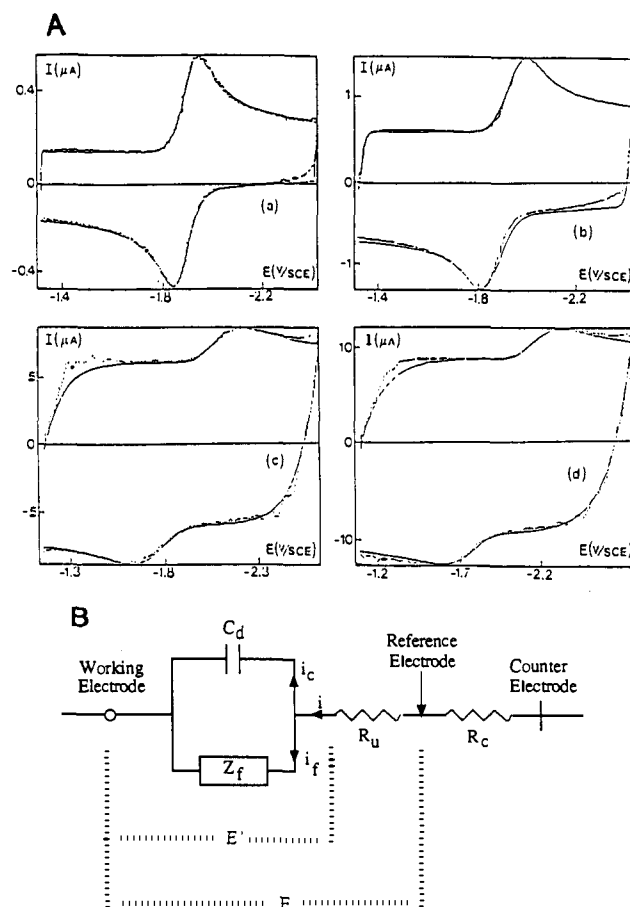


**Figure 1.** (A) Cyclic voltammogram of anthracene (10 mM) in acetonitrile + 0.6 M  $\text{Et}_4\text{NBF}_4$  at a 5- $\mu\text{m}$ -diameter gold disk electrode. Temperature: 25 °C. Scan rates: 22 100 (a), 113 400 (b), 1 191 000 (c), and 1 724 000 (d) V/s. (B) Equivalent circuit of a three-electrode electrochemical cell. Key:  $R_u$ ,  $R_c$ , resistances comprised between the reference electrode and the working and counter electrodes, respectively;  $C_d$ , double-layer capacitance;  $i$ , total current;  $i_f$ , faradaic current;  $i_c$ , double-layer charging current.

sponse time  $R_u C_d$  of the portion of the cell comprised between the working and reference electrodes

$$i_c = C_d v [1 - \exp(-t / -R_u C_d)] \quad (5)$$

( $v$  = scan rate,  $t$  = time). The plateau height of the double-layer charging current is thus proportional to  $v$  whereas the faradaic current is approximately proportional to the square root of  $v$ . The increase of the potential difference between the cathodic and anodic peaks with the scan rate arises from the interference of the electron-transfer kinetics on one hand but also from the ohmic drop in the resistance  $R_u$  on the other. The rising portion of the double-layer charging current tends to overlap more and more with the faradaic response as the scan rate is increased for the following reasons. Displaying, for example, the voltammogram as a current-potential curve as done in Figure 1A, the rising portion of the double-layer charging current spreads out proportionally to the scan rate since  $R_u C_d$  is independent of the scan rate. On the other hand, the faradaic cathodic peak shifts in the same direction as a result of the increase of the ohmic drop  $R_u i$  with the scan rate. It shifts however less since the faradaic current is roughly proportional to the square root of  $v$ . Thus, as the scan rate is increased in the purpose of achieving larger diffusion rates, it becomes more difficult to extract accurate kinetic information from the current-potential curves.

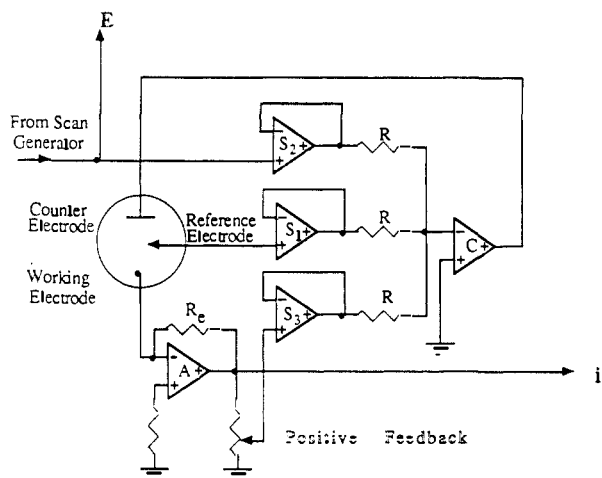


**Figure 2.** Potentiostat (C,  $S_1$ ,  $S_2$ ,  $S_3$ ) and current transducer (A) equipped with positive-feedback  $iR$  compensation. Key:  $R_e$ , sampling resistor; P, voltage divider; R, adder resistors.

It follows that decreases of both the cell response time and the ohmic drop are beneficial when high scan rates are sought. The strategies employed to overcome, at least partly, these problems before the popularization of ultramicroelectrodes were based on positive-feedback compensation of the cell resistance.<sup>9-11</sup> Figure 2 illustrates the principle of the method where a voltage proportional to the current is subtracted, at the level of the reference electrode, from the voltage issued from the function generator. This amounts to subtracting a fraction  $\beta$  of the sampling resistor  $R_e$  to the solution resistance  $R_u$  comprised between the reference and working electrodes. When attempting to annul the remaining resistance  $\Delta R_u = R_u - \beta R_e$ , sustained oscillations appear, making any measurement impossible. The apparatus indeed behaves approximately as a self-inductance, whose value depends upon the bandwidth of the amplifiers (with the operational amplifiers currently used in positive-feedback  $iR$  compensation setups, of the order of a fraction of millihenry). The value of  $R_u$  can be derived from the sustained oscillatory behavior, and hence that of the remaining resistance  $\Delta R_u$ , under conditions where measurements can be performed, i.e., selecting  $\beta$  so as the current response to show only a few damped oscillations not overlapping too seriously with the faradaic wave.  $\Delta R_u$  values of the order of 100  $\Omega$  are found in current practice. Since with millimetric electrodes the double-layer capacitance is of the order of  $10^{-7}$  F, the cell response times are of the order of 10  $\mu$ s. This allows maximal scan rates of the order of a few thousands volts per second to be used. At these scan rates, still using millimetric electrodes, the residual  $iR$  drop resulting from the minimal uncompensated resistance is of the order of 100 mV and the distortion brought about by the potentiostat and current measurer is of the order of a few millivolts. The experimental data can then be mathematically corrected from the effect of the remaining ohmic drop from the equivalent circuit shown in Figure 1B.<sup>12</sup> Careful evaluation of these various effects showed,<sup>13</sup> with a convolution transformation<sup>14</sup> as testing procedure, that reliable results can be obtained up to ca. 2500 V/s.

Another way to decrease both the cell response time and the ohmic drop is to decrease the diameter  $d$  of the working electrode. The resistance between the working and reference electrodes is mostly concentrated in the

close vicinity of the former because of its small size as compared to the counter electrode. It increases as the diameter of the working electrode decreases, approximately as  $1/d$ . Since, on the other hand, the double-layer capacitance  $C_d$  and the total current  $i$  are proportional to the surface area of the electrode, i.e., to  $d^2$ , the cell response time  $R_u C_d$  and the ohmic drop  $R_u i$  both decrease as the electrode is made smaller. If the electrode diameter passes from 1 mm to 10  $\mu$ m, the cell response time and the  $iR$  drop decrease by a factor of 100. These are the reasons why the use of ultramicroelectrodes, first introduced by Wightman et al.<sup>15</sup> in cyclic voltammetry and by McCreery et al.<sup>16,17</sup> in spectroelectrochemistry, has allowed quite significant improvements in the achievement of high diffusion rates in fast-scan or step electrochemical techniques. The application of ultramicroelectrodes to slow-scan techniques also allows the achievement of rather high diffusion rates, but for quite different reasons. With such small electrodes, diffusion ceases to be linear to become approximately spherical in the conventional range of scan rate values. A steady-state current is then obtained, and the diffusion rate is the higher the smaller the electrode. This other application of ultramicroelectrodes<sup>18,19</sup> will not be dealt with in the following discussion.

## B. Instrumentation and Procedures

Since very short measurement times are sought, particular care must be exercised for minimizing the various possible sources of distortion of the current-potential curves by the instrument. Appropriate function generators and digital oscilloscopes (minimal sampling time in the nanosecond range) are available from commercial sources. The critical sections of the experimental setup are the ultramicroelectrode itself and the potentiostat and current transducer instrument.

The procedures to be used for preparing and polishing the ultramicroelectrodes are described in detail in ref 18. Good sealing of the wire in the supporting glass tube, avoiding the creeping of the solution between the wire and the glass wall, is of particular importance. Stray capacitances in all sections of the system must be minimized. In this connection, procedures for minimizing the capacitance between the internal portion of the ultramicroelectrode wire and the solution through the glass wall have been described.<sup>20</sup>

Potentiostat-current transducer setups allowing the recording of faradaic current-potential curves negligibly affected by instrument distortion up to scan rates in the kilovolt,<sup>21-23</sup> the tens kilovolt,<sup>24</sup> and the megavolt<sup>25,26</sup> per second range with a two-electrode or three-electrode configuration have been described in detail. Deconvolution procedures have been proposed<sup>22,23,27</sup> for correcting the current responses from instrument distortions, allowing the extension of the useable range of scan rates from kilovolts per second to  $10^6$  V/s. Although this is a valuable improvement, direct extension of the instrument capabilities seems preferable. In the latter case it is conceivable that correction of instrument distortion could further improve the performances. Figure 3 shows the potentiostat and current transducer setup used in the megavolt per second range of scan rates.<sup>26</sup> As far as bandwidth limitations are concerned, the critical section of the instrument is the current

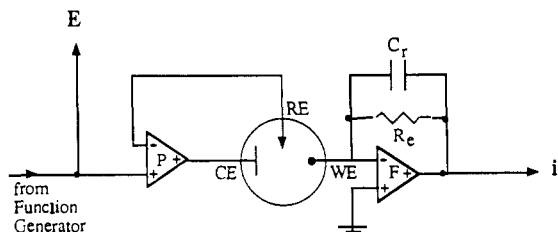


**Figure 3.** Potentiostat and current transducer for cyclic voltammetry at ultramicroelectrodes in the megavolt per second range of scan rates. Key: WE, RE, CE, working, reference, and counter electrodes respectively; P, potentiostat (200 MHz); F, current follower (200 MHz);  $C_s$ , stabilizing capacitance.

transducer rather than the potentiostat. The presence of stray capacitances of various origins (ultramicroelectrode, operational amplifiers, wiring...) induces the appearance of an oscillatory behavior that impedes any investigation of the faradaic response. This is the reason why a stabilizing capacitance is introduced in the current transducer circuit so as to make the best possible compromise between damping of the oscillations and keeping of the largest possible bandwidth.

At such high scan rates, the effect of ohmic drop, even though diminished thanks to the use of an ultramicroelectrode instead of a conventional microelectrode, is by no means negligible. One strategy for eliminating this effect so as to extract the desired kinetic information out of the raw data consists of simulating the cyclic voltammograms taking into account, besides the kinetic laws appropriate for the reaction under study, the effect of ohmic drop in the resistance between the working and reference electrodes and of the double-layer charging process. The pertinent equations to be used in this connection are the following,<sup>12,24-26</sup> using the equivalent circuit of Figure 1B

$$\begin{aligned} i &= i_f + i_c & E' &= E + R_u(i_f + i_c) \\ i_c &= -C_d dE'/dt \end{aligned} \quad (6)$$

to be combined with the diffusion equations (possibly containing homogeneous kinetic terms) and initial and boundary conditions describing the faradaic process.  $E$  is a function of time depending on the particular electrochemical technique employed. For example, during the cathodic scan of a cyclic voltammetry experiment,  $E = E_1 - vt$  ( $E_1 =$  initial potential). Post factum or on-line<sup>21</sup> (by difference with the current obtained simultaneously with a solution containing only the supporting electrolyte) subtraction of the double-layer charging current from the total current response may improve the accuracy of current measurements because the full Y-scale of the recorder can then be used to display a current that mostly contains the faradaic response. It does not however constitute an accurate treatment of the effect of ohmic drop and double-layer charging on the faradaic response since, as seen in Figure 1, "under" the faradaic wave, the double-layer charging current is not constant and equal to its plateau value. The above equations provide a rigorous solution to the problem.

Since high scan rate applications are dealt with, diffusion can be regarded as linear in the preceding treatment because the diffusion layer thickness is then smaller than the ultramicroelectrode radius even though this is small. Although more refined analyses of diffusion at microdisks must be used when dealing with

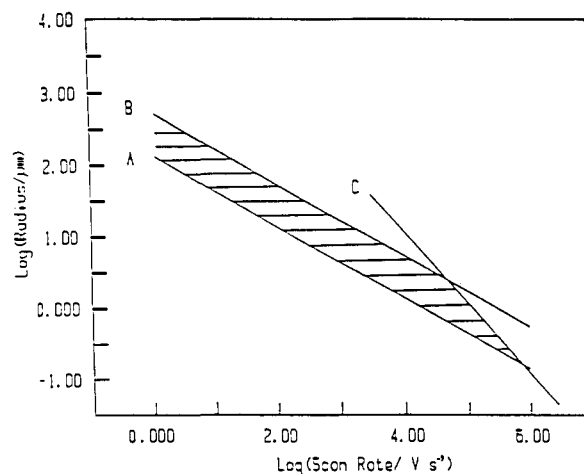


**Figure 4.** Practical working region in cyclic voltammetry at ultramicroelectrodes for negligible nonlinear diffusion effects 3% on peak currents (above line A), negligible (within 3-mV)  $iR$  drop (below line B), and negligible ( $R_u C_d Fv/RT < 1.0$ ) overlap between the rising portion of the double-layer charging current and the faradaic wave (left of line C).

slow-scan applications,<sup>18</sup> it can be regarded as approximately spherical for the present purposes. At low scan rates, the spherical diffusion plateau current is<sup>28</sup>

$$i_{\text{sph}} = \frac{FSC^0D}{r_0} \quad (7)$$

( $S =$  electrode surface area,  $D =$  diffusion coefficient,  $r_0 =$  disk radius) whereas the limiting behavior at high scan rates would be a linear diffusion peak current expressed as

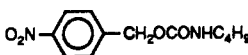
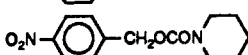
$$i_{\text{lin}} = \gamma FSC^0D^{1/2} \left( \frac{Fv}{RT} \right)^{1/2} \quad (8)$$

( $v =$  scan rate,  $\gamma =$  numerical factor depending upon the faradaic kinetics and mechanism). In the case of slow charge transfer and significant ohmic drop,  $\gamma$  is typically of the order of 0.3. It follows, e.g., that the condition  $i_{\text{sph}}/i_{\text{lin}} \leq 0.05$  will be fulfilled (at room temperature, with  $D = 10^{-5} \text{ cm}^2/\text{s}$ ) above 1000 V/s for  $r_0 = 10 \mu\text{m}$  and above 100 000 V/s for  $r_0 = 1 \mu\text{m}$ . Since, as discussed in the following, an advisable strategy is to decrease the electrode size as shorter and shorter measurement times are sought, the linear diffusion approximation can be safely used for most practical purposes.

Figure 4 shows the range of useable scan rates in relation to electrode radius for the fulfillment of the condition that the ohmic drop and the effect of nonlinear diffusion are both negligible.<sup>29</sup> The line corresponding to achievement of the condition that the double-layer charging current has reached its plateau value before the start of the faradaic wave is also shown in the figure. Particular values of the medium resistivity, the diffusion coefficient, and double-layer capacitance were used for this estimation, but it can be readily adapted for other values of these parameters.

Typical examples of the application of the procedure described above, in the case where ohmic drop is not negligible and diffusion can be regarded as linear, are shown in Figure 1A for the reduction of anthracene. Others can be found in refs 24 and 26 and with a slightly different simulation procedure in ref 29 (in which, also, the linear Butler-Volmer kinetic law is replaced by the Marcus-Hush quadratic equation).

TABLE I. Measurements of Fast Heterogeneous Electron-Transfer Kinetics by Cyclic Voltammetry at Ultramicroelectrodes<sup>a</sup>

substrate (oxidized form)	solvent	scan rate, V/s	electrode (diam, $\mu\text{m}$ )	$k_s^p$ , cm/s	ref
anthracene	acetonitrile	$5 \times 10^2$ – $10^4$	Au (6.5)	$3.5 \pm 0.6$	15
		$10^2$ – $10^3$	Pt (10)	2.6	33
		$2 \times 10^4$ – $2 \times 10^6$	Au (5)	$3.8 \pm 0.5$	25, 26
		$10^4$ – $10^5$	Au (2.5, 8.5)		30
		$2 \times 10^4$ – $2 \times 10^5$	Au (5, 17)		31
anthraquinone	DMF	$2 \times 10^4$ – $3 \times 10^5$	Au (5)	$3.3 \pm 0.2$	24
	acetonitrile	$5 \times 10^2$ – $10^4$	Au (6.5)	$1.8 \pm 0.4$	15
naphthoquinone		$10^2$ – $10^3$	Pt (10)	1.5	33
		$5 \times 10^2$ – $10^4$	Au (6.5)	$0.7 \pm 0.1$	15
benzoquinone		$5 \times 10^2$ – $10^4$	Pt (5)	$0.6 \pm 0.1$	15
		$5 \times 10^2$ – $10^4$	Au (6.5)	$0.4 \pm 0.1$	15
		$5 \times 10^2$ – $10^4$	Pt (5)	$0.2 \pm 0.05$	15
		$10^2$ – $10^3$	Pt (10)	0.15	33
		$10^2$ – $10^3$	Pt (10)	0.2	33
		$10^2$ – $10^3$	Pt (10)	0.3	33
nitromesitylene <sup>b</sup>	DMF	$3 \times 9 \times 10^3$	Hg (50)	0.045	29
		$10^2$ – $10^3$	Pt (10)	1.1	33
ferrocenium		$5 \times 10^2$ – $10^4$	Pt (5)	$1 \pm 0.4$	22
		$5 \times 10^2$ – $10^4$	Hg (5.5)	$1 \pm 0.6$	22
		$5 \times 10^2$ – $10^4$	Au (5)	$3 \pm 1$	22
		$5 \times 10^2$ – $10^4$	Au (5)	2.5	22
		$5 \times 10^2$ – $10^4$	Au (5)	3.5	22
Ru(bpy) <sub>3</sub> <sup>2+/+</sup>	H <sub>2</sub> O	$5 \times 10^2$ – $10^4$	Au (5)	$0.5 \pm 0.1$	22
Ru(bpy) <sub>3</sub> <sup>+ /0</sup>		$5 \times 10^2$ – $10^4$	Au (5)		22
Ru(NH <sub>3</sub> ) <sub>3</sub> <sup>3+ /2+</sup>		$5 \times 10^2$ – $10^4$	Au (5)		22

<sup>a</sup>Temperature ranging from 20 to 25 °C unless otherwise stated. <sup>b</sup>–50 °C.

Simulation of the effect of the instrument (Figure 3) on the current–potential curves, using values of its characteristic parameters derived from a dummy cell study, showed that, in the megavolt per second range, it amounts to a small and easily correctable shift of the potential scale.<sup>26</sup>

Another strategy for correcting the effect of ohmic drop is positive-feedback compensation just as in the case of conventional microelectrodes. It has obviously the advantage of simplicity as compared to the previous approach. Some decrease of the maximal useable scan rates is however anticipated owing to the introduction of an additional operational amplifier taking care of the positive-feedback operation. In spite of these difficulties, the feasibility of positive-feedback compensation at ultramicroelectrodes has been demonstrated up to ca. 20 000 V/s with a quite convenient three-electrode configuration.<sup>30</sup> A factor of about 10 in scan rate can be gained thanks to the use of current instead of potential feedback operational amplifiers, with however a two- rather than a three-electrode configuration (Figure 5).<sup>31</sup>

Convolution of the cyclic voltammetric current responses by the linear diffusion characteristic function<sup>14</sup>  $(\pi t)^{-1/2}$  has been used in several instances to process the cyclic voltammetric data.<sup>22,24</sup>

On the other hand, potential step and double potential step techniques are quite valuable for the investigation of coupled homogeneous reactions because the measurements can be made independent of the ohmic drop and of the heterogeneous electron-transfer kinetics, as discussed in the following section. They have been used with the same type of potentiostat and current transducer instrumentation.<sup>32</sup>

### C. Fast Heterogeneous Electron Transfer

In Table I the available data concerning determination of standard rate constants of fast heterogeneous

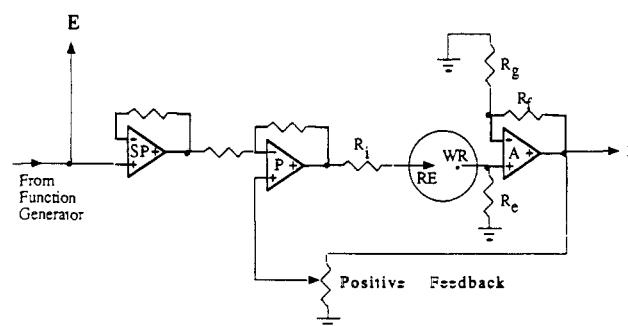


Figure 5.  $iR$  compensation up to 200 000 V/s. Key: WE, working electrode; RE, reference electrode;  $R_s$ , sampling resistor;  $R_f$ , feedback resistor;  $R_g$ , gain resistor;  $R_i$ , isolation resistor; A, current-measuring amplifier; P, summing amplifier; SP, booster amplifier.

electron transfers from the anodic to cathodic peak potential distance in cyclic voltammetry are gathered. Given the system, the peak distance increases with the scan rate, which contributes to improve the accuracy of the rate constant determination. Adverse effects upon going to the very high scan rates originate in the bandwidth limitations of the instrument, in the effect of stray capacitances, and in the statistical and systematic errors in the elimination of the ohmic drop and double-layer charging current through simulation procedures owing to the approximate character of the underlying assumptions (validity of the equivalent circuit, the diffusion law, and large number of adjustable parameters). The best operating conditions in this connection are probably to use the largest possible portion of the scan rate range, from kilovolts to megavolts per second now available for investigating quite fast electron transfers. Such a systematic evaluation of the technique is however still awaited. The anthracene/anthracene anion radical couple in acetonitrile or in DMF has become one of the most popular systems for

TABLE II. Investigation of Homogeneous Follow-Up Reactions by Fast Electrochemical Techniques at Ultramicroelectrodes<sup>a</sup>

no.	system	scan rate, V/s	electrode (diam, $\mu\text{m}$ )	lifetime, <sup>b</sup> s	ref
1	oxidation of polyalkylbenzenes in trifluoroacetic acid	$2 \times 10^2$ – $2 \times 10^3$	Au (13)	c	35
2	oxidation of anthracene and 9,10-diphenylanthracene in acetonitrile, methylene chloride, dimethoxyethane	$2 \times 10^2$ – $10^4$	Au (13) Pt (5)	c	36
3	oxidation of aromatic hydrocarbons in DMF	$3 \times 10^3$ – $2 \times 10^4$	Au (17, 5)	c	37
4	anion radical quinones/dinegative quinones in protic solvents at high pH	$2 \times 10^2$	Hg (5.5)	c	38
5	oxidation of ascorbic acid in $\text{H}_2\text{O}$	$10$ – $10^3$	Hg (5)	$10^{-3}$	39
6	oxidation of pyrrole and substituted pyrroles in acetonitrile (first stage of electropolymerization process)	$10^3$ – $2 \times 10^4$	Pt (5, 10) Au (17)	$2 \times 10^{-3}$ – $3 \times 10^{-5d}$	40
7	reductive dimerization of 2,6-diphenylpyrilium cation in acetonitrile	$2.5 \times 10^5$	Pt (5)	$5 \times 10^{-8e}$	41
8	isomerization of 1,1'-dimethylbianthrone and dixanthylene in DMF	$2 \times 10^2$ – $5 \times 10^3$ $10^3$ – $3 \times 10^4$	Pt (5) Hg (12.5)	$10^{-2}$ – $10^{-4}$	42 29
9	cleavage of electrochemically generated aromatic halide anion radicals in DMF	$10^5$ – $4 \times 10^5$	Au (5)	$10^{-5}$ – $10^{-6}$	43
10	cleavage of electrochemically generated aromatic halide anion radicals in acetonitrile	$10^{-2}$ – $5 \times 10^5$	Au, Pt (5, 10, 100)	$10^{-1}$ – $2 \times 10^{-6}$	44
11	reductive dimerization of 4-methyl-4- <i>tert</i> -butylpyridinium in DMF	<i>f</i> $10^{-3}$ – $3 \times 10^{-6}$	Au (5, 17)	$6 \times 10^{-5}$ – $10^{-5}$	32
12	reductive dimerization of 10-methylacridinium ( $\text{NAD}^+$ analogue) in acetonitrile	<i>f</i> $10^{-4}$ – $2 \times 10^{-5}$		$2 \times 10^{-5}$	45
13	ECE-DISP oxidation of 10-methylacridane ( $\text{NADH}$ analogue) in acetonitrile deprotonation of the cation radical by pyridine and substituted pyridines	$10^3$ – $10^5$ <i>f</i> $10^{-4}$ – $2 \times 10^{-5}$	Au (5, 17)	$10^{-2}$ – $3 \times 10^{-5}$	45

<sup>a</sup>By cyclic voltammetry unless otherwise stated. <sup>b</sup> $=1/k$  for first-order kinetics,  $=1/(k[\text{substrate}])$  for second-order kinetics.

<sup>c</sup>Determination of the substrate/intermediate standard potential with no investigation of the decay kinetics of the intermediate.

<sup>d</sup>Determination of the standard potential and approximate estimate of the cation radical lifetime. <sup>e</sup>Approximate determination of the dimerization rate constant from the standard potential estimated at high scan rate and the peak potential at low scan rates (at 20 °C:  $E_p = E^\circ - 0.047 + 0.0194 \log k^2$ ). <sup>f</sup>Double-potential step; the numbers below are the step durations.

testing the performance of fast-responding instruments. It is indeed one of the fastest electron-transfer processes one can think of since very little reorganization, if any, is involved owing to its aromatic character; its solvent fluctuational reorganization is also small because of its large size. It follows that one is likely to be able to determine the rate constant of any fast heterogeneous electron-transfer process using cyclic voltammetry at ultramicroelectrodes in view of the very large scan rates that can be achieved. Note for example, in this connection, that for anthracene in DMF it was found<sup>24</sup> that  $k_S^{\text{ap}} = 3.3 \pm 0.2 \text{ cm/s}$  (heterogeneous rate constant uncorrected for the double-layer effect) to be compared with  $k_S^{\text{ap}} = 5 \pm 2 \text{ cm/s}$  as obtained, by the impedance technique with a conventional microelectrode at the upper edge of its range of applicability.<sup>34</sup>

#### D. Fast Homogeneous Coupled Reactions

Quite a few examples now exist in the literature of the use of ultramicroelectrode techniques for investigating electrochemical processes involving a fast homogeneous follow-up reaction. They are summarized in Table II. In several cases, the main objective of the investigation was to detect the fast-decaying one-electron reduction (or oxidation) intermediate by observing that the initially irreversible cyclic voltammetric pattern converts to a one-electron reversible wave upon increasing the scan rate. In such cases, the standard potential of the substrate/intermediate redox couple was also determined. There are however an increasing number of reactions in which the rate constant of the rate-determining step of the homogeneous follow-up process has been measured. The shortest reachable lifetimes in this respect are of the order of fractions of microseconds in the present state of the art.

The procedure for determining the rate constant by cyclic voltammetry is illustrated in Figure 6 with the example of the reduction of 9-bromoanthracene in

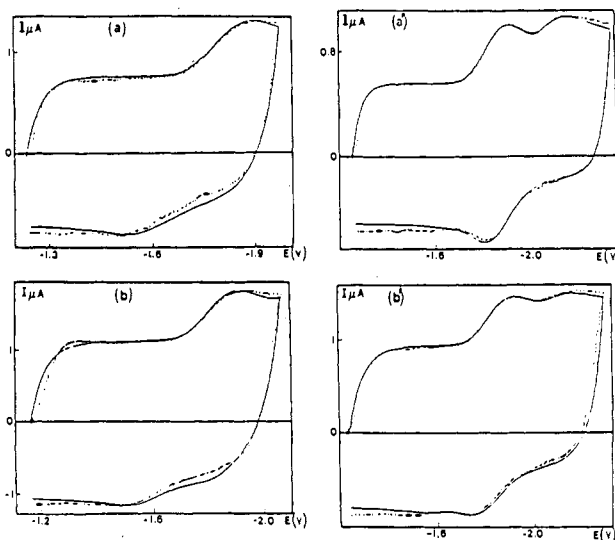
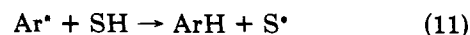
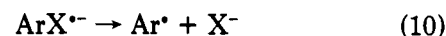
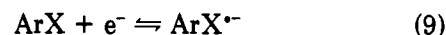
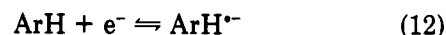


Figure 6. Cyclic voltammetry of 9-bromoanthracene (10 mM) in DMF + 0.4 M  $\text{Et}_4\text{NBF}_4$  at a 5- $\mu\text{m}$ -diameter gold disk electrode, encompassing the first wave (a, b) and both waves (a', b'). Scan rates: 15 000 (a), 228 000 (b), 113 000 (a'), 182 000 (b'). Key: points, experimental data; solid line, simulated curves.

DMF.<sup>43</sup> The reaction taking place at the first cathodic wave involves an EC mechanism



and at the second wave



The simulation procedure is similar to that described in the preceding section for the reduction of anthracene, except that the kinetic terms corresponding to the ho-

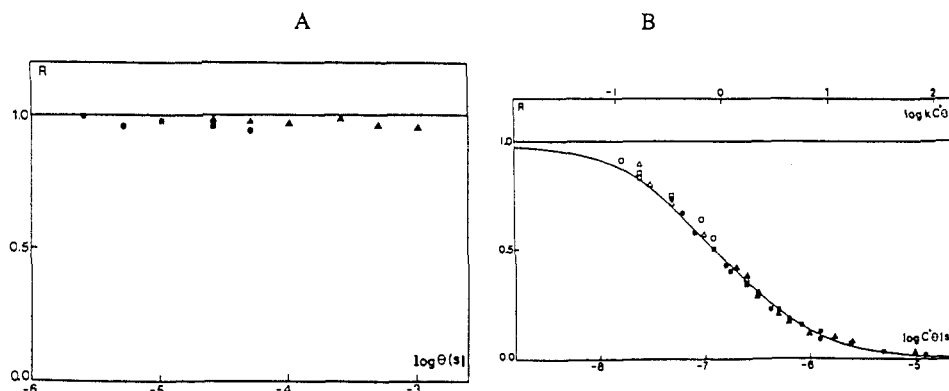


**Figure 7.** Double potential step chronoamperometry of anthracene (A) and of 1-methyl-4-*tert*-butylpyridinium (B) in DMF + 0.4 M  $\text{NET}_4\text{BF}_4$  at 5- and 17- $\mu\text{m}$ -diameter gold disk electrodes. Variation of current ratio  $\bar{R}$  (eq 16) with inversion time  $\theta$  at 25 °C: (A) anthracene concentration 10 mM 5 (■) and 17 (▲)  $\mu\text{m}$  electrodes; (B) 1-methyl-4-*tert*-butylpyridinium at 2.5 (●), 5 (○, ■), 10 (△, ▲) mM concentrations with 5 (open) and 17 (closed)  $\mu\text{m}$  electrodes. Full line indicates theoretical variation of  $\bar{R}$  with  $k[\text{substrate}]\theta$  for a radical-radical coupling mechanism.<sup>2</sup>  $k = (6.4 \pm 0.5) \times 10^6 \text{ M}^{-1} \text{ s}^{-1}$ .

homogeneous reactions (10, 11, 13) are introduced in the diffusion equations. There are also more adjustable parameters, besides  $R_u$  and  $C_d$ , that can be derived from the double-layer charging current at the foot of the first faradaic wave: the standard potentials, standard rate constants, and transfer coefficient for the two heterogeneous electron-transfer steps (9, 12), for which the source of information is the location and width of the first cathodic wave and of the anodic wave and their peak separation (9) and the location and width of the second cathodic wave for (12) and the rate constant of the homogeneous chemical step (10), i.e., what is sought (step 13 can be considered as being at the diffusion limit resulting from the standard potential separation of the two intervening redox couples). In other words, there are more adjustable parameters, but there are also more exploitable features in the cyclic voltammograms. It is seen that there is satisfactory agreement between the experimental and simulated curves at the various investigated scan rates, encompassing the two cathodic waves or only the first one. The rewarding counterpart of the tedium of such simulation procedures is that both the rate constant of the homogeneous follow-up step is obtained and also the kinetic and thermodynamic characteristics of the two heterogeneous electron-transfer steps are determined.

If the mechanisms and rate constants of the homogeneous chemical steps are solely sought, double potential step techniques offer a much simpler alternative to cyclic voltammetry since the current responses can be freed from the effects of  $iR$  drop and charge-transfer kinetics. This approach is illustrated in Figure 7 with the example of the reduction of the 1-methyl-4-*tert*-butylpyridinium cation in DMF.<sup>32</sup> A first step to be taken when applying this technique is to investigate the time window in which the above conditions are actually achieved. At the short time edge one must make *sure* that the double-layer charging current during the forward step

$$i_c = \frac{\Delta E}{R_u} \exp\left(-\frac{t}{R_u C_d}\right) \quad (14)$$

and during the reverse step

$$i_c = -\frac{\Delta E}{R_u} \left[ 1 - \exp\left(-\frac{\theta}{R_u C_d}\right) \right] \exp\left(-\frac{t-\theta}{R_u C_d}\right) \quad (15)$$

( $\Delta E$  = amplitude of the potential step,  $\theta$  = inversion time) interferes negligibly in the faradaic response and also that the step reaches the plateau of the wave, i.e., a potential region where the charge-transfer kinetics interferes negligibly. The most convenient test in this connection is to use another substrate of similar diffusion coefficient giving rise to a one-electron reversible response in the same medium (anthracene in Figure 7A). The range of time in which the normalized current ratio

$$R = \frac{i(2\theta)/i(\theta)}{[i(2\theta)/i(\theta)]_{\text{diffusion}}} \quad (16)$$

is effectively equal to 1 thus defines the useable time window. Within the time window so defined, the data obtained for the reduction of 1-methyl-4-*tert*-butylpyridinium adhere satisfactorily with the theoretical predictions for a radical-radical coupling mechanism.<sup>2</sup> On these bases, the performances of the technique in terms of shortest attainable lifetimes and relative precision of their determination can be more generally estimated to be the following:<sup>32</sup>

$R_{\text{max}}$	lifetime, $\mu\text{s}$	rel error, %
0.30	1.2	10
0.20	0.6	20
0.10	0.3	40
0.05	0.1	100

### III. Indirect Methods: Redox Catalysis

#### A. Indirect vs Direct Methods

The principle of direct electrochemical kinetic methods, such as those discussed in the preceding section, consists of creating a competition between the reaction of interest, electron transfer at the electrode or coupled homogeneous steps, and the diffusion of the intervening species to and from the electrode surface. This diffusion process that plays the role of a kinetic reference may be linear as when using conventional microelectrodes or ultramicroelectrodes in their fast-scan or fast-step applications or quasi-spherical as in the slow-scan applications of ultramicroelectrodes. In the first case, fast diffusion rates, allowing fast reactions to be investigated, are obtained by playing directly with the time, i.e., by imposing to the system a shorter and



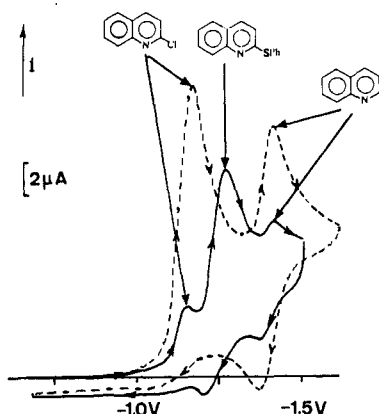
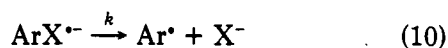
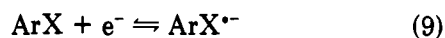


**Figure 8.** Cyclic voltammetry of 2-chloroquinoline (2.5 mM) in  $\text{NH}_3(\text{l}) + 0.1 \text{ M KBr}$  at  $-40^\circ\text{C}$  in the absence (---) and presence (—) of benzenethiolate (56 mM). Scan rate: 0.2 V/s.

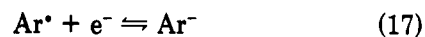
shorter time perturbation. In the second case, one plays with space to achieve similarly an increase of the diffusion rate by forcing a geometrical concentration of diffusion lines. We will see in the following text that one of the most efficient indirect methods, the redox catalysis method, bears some resemblance with the latter method pushing it to a limit: What plays the role of the small electrode is then a molecule.

More generally, in indirect electrochemical kinetic methods, a competition is created between the reaction of interest and another chemical reaction, the rate constant of which is known independently and can thus serve as a kinetic reference instead of the diffusion to and from the electrode in direct methods. Various approaches can be employed depending on what observable is chosen. In the redox catalysis method, already evoked in the Introduction and described in detail in the two next sections, an electrical observable is used, viz., the current flowing through the electrode. This is also the case, in a more direct fashion, with systems in which competition between the investigated and reference reactions changes the overall electron stoichiometry according to which the substrate is reduced (or oxidized).

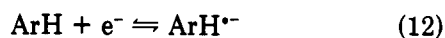
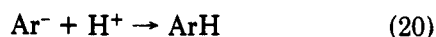
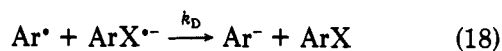
Let us take, as an example illustrating the latter point, reduction of aryl halides in the presence of a nucleophile (Figure 8) giving rise to an electrochemically induced<sup>2,8-8,46</sup>  $\text{S}_{\text{RN}}1$ <sup>47</sup> aromatic substitution



electron-transfer reduction pathway



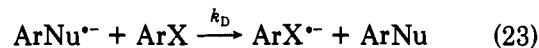
and/or



nucleophilic attack pathway



and/or



In the absence of nucleophile, the voltammogram exhibits a first irreversible two-electron reduction wave corresponding to the one-electron formation of the  $\text{ArX}^{\bullet-}$  anion radical (9). Its decomposition leads to the aryl radical  $\text{Ar}^{\bullet}$  (10). This is then reduced at the electrode (17) or in the solution (18), ultimately yielding the hydrogenated hydrocarbon  $\text{ArH}$  (20), the reversible reduction of which into its anion radical (12) is responsible for the second, one-electron, reversible wave. Upon addition of the nucleophile, these two waves decrease while a third, one-electron, reversible wave appears and increases accordingly, corresponding to the reversible reduction of the substituted product into its own anion radical as checked with an authentic sample. After its initial formation at the electrode surface, the  $\text{ArX}^{\bullet-}$  anion radical diffuses toward the solution while decomposing into the aryl radical  $\text{Ar}^{\bullet}$ , which then reacts with the nucleophile, yielding the  $\text{ArNu}^{\bullet-}$  anion radical (21). This is eventually oxidized into the final substitution product  $\text{ArNu}$  at the electrode surface (22) or in the solution (23). The overall reaction (24) does not consume electrons. These merely play the role of a catalyst for the substitution process. Thus, if no other reactions were to occur competitively with the  $\text{S}_{\text{RN}}1$  process, the  $\text{ArX}$  waves should have decreased to zero. This is what happens eventually when the nucleophile concentration is increased. On the other hand, at the small scan rates employed, the overall system is chemically irreversible, indicating that the various chemical steps take place in a thin reaction layer adjacent to the electrode surface, much thinner than the diffusion layer. Thus, at intermediate concentrations of the nucleophile, when the  $\text{ArX}$  waves have not yet reached zero, their height is the reflection of a competition between the substitution process (right-hand side of the above scheme) and the various steps in which the radical is reduced (left-hand side of the above scheme). The competition may take place within an ECE context (reactions 17 and 22) or within a DISP context (reactions 18, 19, and 23). Whether one or the other possibility predominates primarily depends upon the rates at which  $\text{ArX}^{\bullet-}$  decomposes and the ensuing  $\text{Ar}^{\bullet}$  radical reacts with the nucleophile. If these reactions are very rapid,  $\text{ArNu}^{\bullet-}$  is formed close to the electrode surface and will thus predominantly be oxidized into  $\text{ArNu}$  there. Conversely, if they are less rapid, the oxidation of  $\text{ArNu}^{\bullet-}$  will predominantly take place in the solution. In the first case the height of the first cathodic peak is a known decreasing function of the rate constant ratio  $k/k_{\text{Nu}}$  whereas in the second, which prevails with the reaction shown in Figure 8, it is a known decreasing function of the rate constant ratio  $k_{\text{D}}[\text{ArX}](Fv/RT)^{1/2}/k^{1/2}k_{\text{Nu}}[\text{Nu}^-]$  (reactions 18 and 19 are at the diffusion limit in view of the standard potential difference between the intervening redox couples). Thus, if one of the two rate constants is known from inde-

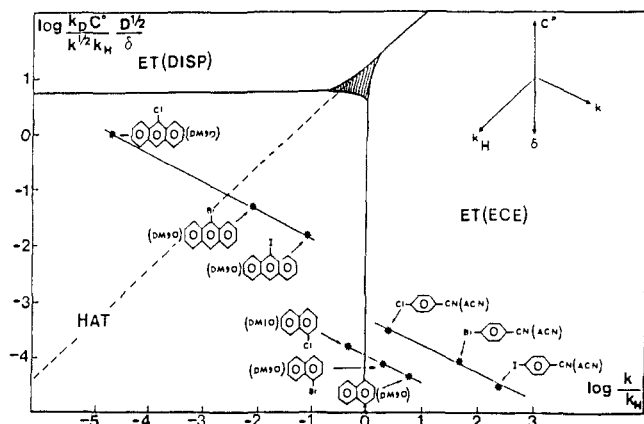
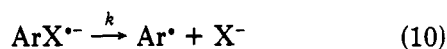
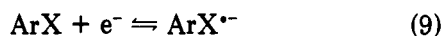


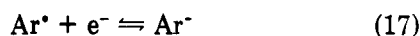
**Figure 9.** Competition between H atom transfer and electron transfer in the reduction of some aryl halides in DMSO and ACN. The symbols are the same as defined in the text.

pendent sources, the other can be derived from this type of experiment.

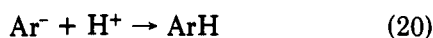
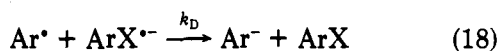
Another valuable observable is the distribution of products in preparative-scale electrolysis in so far it reveals competition between two reactions, one of which is the reaction of interest and the other is known from the independent sources and may thus serve as reference reaction. As an example, the reactions following and Figure 9 show the competition taking place in the reduction of aryl halides in H atom donor solvents such as acetonitrile and DMSO.<sup>49</sup>



electron-transfer pathway:



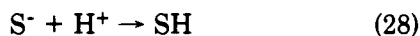
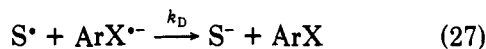
and/or



H atom transfer pathway:



and/or



The product ArH and the electron stoichiometry are the same for both pathways. The use of standard microelectrolytic techniques is thus of little help for unraveling the reaction kinetics. This can be established by preparative-scale deuterium incorporation experiments carried out in heavy water–light organic solvent mixtures and vice versa, based on the fact that water is a much poorer H atom donor than the organic solvent but a much better acid.<sup>49</sup> The yield of ArD obtained in heavy water–light organic solvent mixtures is thus a measure of the electron-transfer pathway, whereas the

yield of RH is a measure of the H atom transfer pathway. The opposite applies to the experiments carried out in light water–heavy organic solvent mixtures. The resulting three-cornered competition is a function of the two parameters

$$\frac{k_D[\text{ArX}]D^{1/2}}{k^{1/2}k_H\delta} \quad \frac{k}{k_H} \quad (29)$$

( $\delta$  = thickness of the diffusion layer,  $D$  = diffusion coefficient). Typical results are displayed in Figure 9 under the form of a diagram showing the zones where one of the competing pathways predominates over the two others (the boundary lines are drawn on the basis of a 50/50 participation of each couple of competing pathways). Among the various experimental parameters that affect the competition, as summarized in the top right-hand corner of Figure 9, the effect of  $k$  is of particular interest. When  $k$  is increased, the system passes from DISP to HAT (H atom transfer) and to ECE. With the 1-naphthalene and 4-benzonitrile derivatives,  $k$  is so large that, for all halogens, the competition practically involves only H atom transfer and heterogeneous electron transfer whereas, with the 9-anthracene derivatives, the reaction passes progressively from a DISP–HAT competition to an ECE–HAT competition. It was found accordingly that, with the latter compounds, deuterium incorporation is a function of the rate of agitation of the solution (the diffusion layer thickness is a decreasing function of the rate of agitation) and of the ArX concentration whereas this is not the case in the 1-naphthalene and 4-benzonitrile series. In each situation the rate constant ratio can be derived from these preparative-scale experiments using the appropriate working curves, thus allowing determination of either  $k$  or  $k_H$  according to the case.<sup>49</sup>

The mathematical analyses and ensuing procedures for the determination of the rate constants from product distribution are available for a large number of mechanism types.<sup>50–60</sup> These analyses are also useful for product optimization in preparative-scale electrolysis (see for example the case of the reduction of  $\text{CO}_2$  in media of low proton availability<sup>61</sup>).

## B. Principle of the Redox Catalysis Method. EC Mechanisms

We start from eq 4 in the Introduction, whereby a mediator P giving rise to a stable reduced form is introduced in the solution. The P/Q couple is selected so as to be electrochemically fast and have a standard potential located positive to the substrate (A) reduction wave (in the following, all reasonings are for a reduction process; they are straightforwardly transposable to the case of oxidation). In the absence of substrate and using for example cyclic voltammetry, the mediator gives rise to a one-electron reversible wave. Addition of the substrate increases the wave and makes it lose its reversibility (Figure 10). This increase of current and loss of reversibility are the observables providing the desired kinetic information concerning the E and the C reactions.<sup>2</sup> According to the competition between the backward electron-transfer step and the C step, the rate-determining step is either the forward electron transfer or the C step with the E step acting as a pre-equilibrium. In the general case, the kinetic term

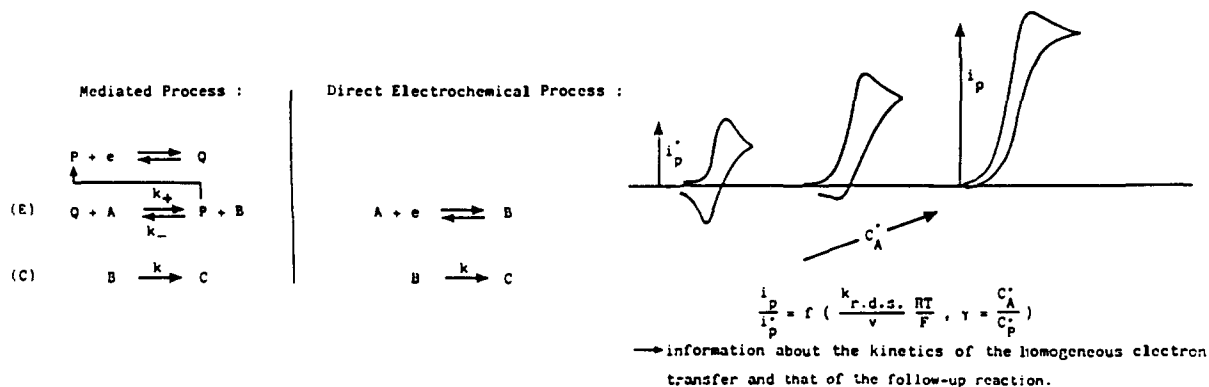


Figure 10. Homogeneous redox catalysis. EC reaction scheme.

to be introduced in the diffusion equations of P, Q, and A is

$$\frac{d[P]}{dt} = -\frac{d[Q]}{dt} = -\frac{d[A]}{dt} = k_+k \frac{[A][Q]}{k_-[P] + k} \quad (30)$$

The kinetic control by the forward E step

$$\frac{d[P]}{dt} = -\frac{d[Q]}{dt} = -\frac{d[A]}{dt} = k_+[A][Q] \quad (31)$$

is achieved when  $k_-[P]_0 \ll k$ . Conversely, when  $k_-[P]_0 \gg k$ , C is the rate-determining step:

$$\frac{d[P]}{dt} = -\frac{d[Q]}{dt} = -\frac{d[A]}{dt} = \frac{k_+k[A][Q]}{k_-[P]} \quad (32)$$

Thus, if it is possible upon increasing the bulk concentration of P,  $[P]_0$ , to pass from (32) to (30) or from (30) to (31), appropriate treatment<sup>62,63</sup> of the cyclic voltammetric data or of the data obtained by any other technique allows the determination of  $k_+$  and  $k_-/k$ . Since  $k_-$  is quite often equal to the diffusion limit (see the next section),  $k_+$  and  $k$ , the rate constant of interest, ensues.

As exemplified in the next section, quite unstable intermediates, having lifetimes down to the nanosecond time range, can be kinetically characterized with these procedures. Why there is such a huge gain in performance as compared to the direct techniques, including ultramicroelectrode fast techniques, is worth some comment. The very principle of the method consists of creating a competition between the reaction of interest, viz., the C step, and a reaction that is at the diffusion limit, the backward E step, which thus serves as a reference process just as in the case of the direct methods discussed earlier. This is reminiscent of the slow-scan application of ultramicroelectrodes where the rate of the diffusion reference process is increased upon going to smaller electrode sizes. In the present case, a "molecular size electrode", so to speak, is used, thus pushing the same principle to an extreme. The "wiring" of this three-dimensional array of "molecular electrodes" (diffusion of P to and of Q from the real electrode) is not as straightforward as with a true electrode putting some restriction on the choice of the mediator couple.

If the C reaction is so fast that the kinetic control is always by the forward E step in the whole available range of  $[P]_0$ , no information concerning the C reaction can be gained from the experimental data. It is however still possible to obtain, in a number of cases, precious information, such as the standard potential and the standard rate constant of the A/B couple. This is

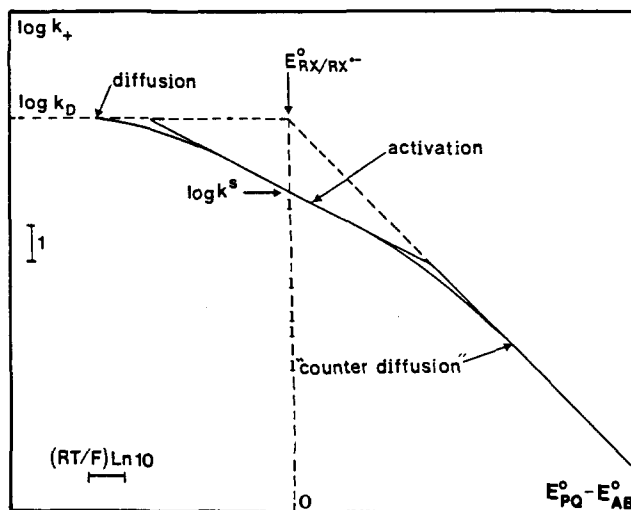


Figure 11. Representation of eq 33 showing the procedure for determining the standard potential  $E^0_{A/B}$  and the standard rate constant  $k^s$ .

feasible when, with a series of mediators of variable standard potentials, it is possible to observe, as far as  $k_+$  is concerned, the transition between activation and "counter diffusion" control, the latter term meaning that the backward electron-transfer step has then reached the diffusion limit. The situation is schematically represented in Figure 11 as a plot of the rate constant of the forward electron transfer against the standard potential difference between the substrate and the mediator, i.e., the driving force of the forward E reaction.<sup>64,65</sup> Three regions appear as to its rate constant, corresponding, from left to right, to diffusion control, activation control, and "counter-diffusion control". In total, the rate constant of the forward electron transfer can be expressed as

$$\frac{1}{k_+} = \frac{1}{k_{+act}} + \frac{1}{k_D} + \frac{1}{k_D \exp\left[\frac{E}{RT}(E^0_{A/B} - E^0_{P/Q})\right]} \quad (33)$$

with

$$\frac{1}{k_{+act}} = \frac{1}{k^s \exp[(\alpha F/RT)(E^0_{A/B} - E^0_{P/Q})]} + \frac{1}{Z \exp[(F/RT)(E^0_{A/B} - E^0_{P/Q})]} \quad (34)$$

( $k^s$  = standard rate constant,  $Z$  = bimolecular collision frequency,  $\alpha$  = transfer coefficient or equivalently the

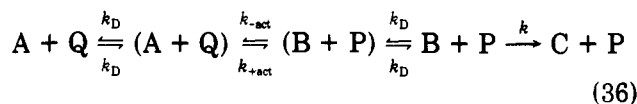
symmetry factor). The (small) variation of  $\alpha$  with the driving force, predicted by Marcus theory of outer-sphere electron transfer<sup>66</sup>—the E reaction is indeed an outer-sphere electron transfer since no bond is broken or formed concertedly with electron transfer—has been omitted for clarity.  $k_D$  is the bimolecular diffusion limit

$$k_D = 4\pi N_A DR \quad (35)$$

according to the Smoluchovski-Debye hard-sphere model ( $N_A$  = Avogadro's constant,  $D$  = twice the average diffusion coefficient of the two reactants,  $R$  = distance of closest approach between their centers).<sup>67-70</sup>

The three successive portions of the plot have slopes equal to zero,  $\alpha F/RT$  and  $F/RT$ , respectively, in terms of a  $\ln k_+$  vs  $E^\circ$  diagram. Thus, if experimental points arising from a family of mediators are available in both the second and third regions, the standard potential and standard rate constant of the investigated redox couple can be obtained as shown in Figure 11.

An explicit assumption in the preceding discussion was that the C step is so fast that the E step is rate-determining. A tacit additional assumption was that it is however not too fast so as for the decay of the B to take place solely outside the diffusion layer surrounding the electron-donor molecule. In other words, the following scheme was assumed



where the parentheses represent the solvent cage.

For faster reactions, the decay of B within the diffusion layer, i.e., within the solvent cage, should be taken into account.<sup>65,71</sup> An extreme situation, opposite to that just discussed, is when the follow-up reaction is so fast that B collapses before having time to diffuse away from the mediator molecule. This is the homogeneous equivalent of the surface follow-up reaction case in electrochemistry. Equation 33 is then replaced by<sup>65</sup>

$$\frac{1}{k_+} = \frac{1}{k_{+act}} + \frac{1}{k_D} + \frac{1}{(kN_A V) \exp\left[\frac{F}{RT}(E^\circ_{A/B} - E^\circ_{P/Q})\right]} \quad (37)$$

where  $V$  is the maximal volume occupied by the A molecules when they are in contact with mediator. In between these two extremes, Q diffuses within the molecular diffusion layer while being converted into C. Then<sup>65</sup>

$$\frac{1}{k_+} = \frac{1}{k_{+act}} + \frac{1}{k_D} + \frac{1}{k_D \left(1 + \frac{Rk^{1/2}}{D^{1/2}}\right) \exp\left[\frac{F}{RT}(E^\circ_{A/B} - E^\circ_{P/Q})\right]} \quad (38)$$

Figure 12a represents the variations of the forward rate constant with the standard potential difference resulting from the combination of eqs 33, 37, and 38 for typical values of the various parameters. The diagram breaks down into three asymptotes with, from left to

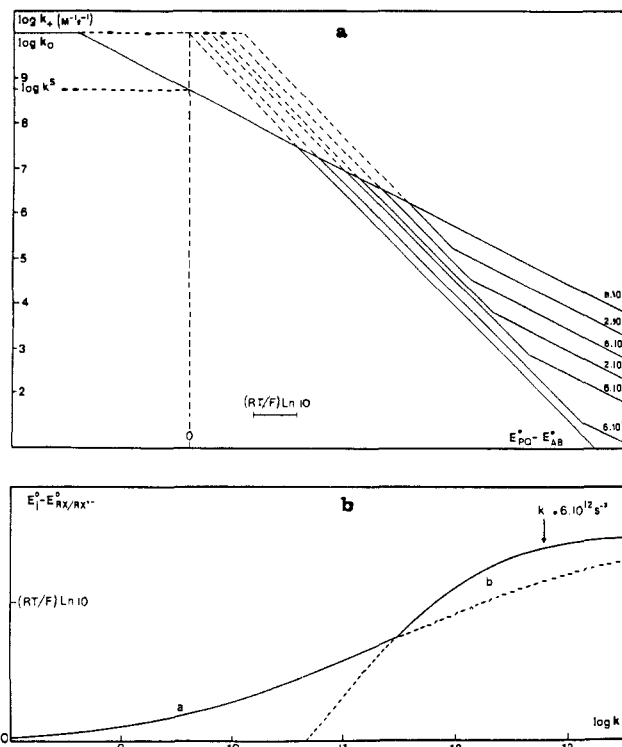


**Figure 12.** (a) Variation of the forward rate constant  $k_+$  with the standard potential difference  $E^\circ_{P/Q} - E^\circ_{A/B}$  as a function of the rate constant of the follow-up reaction  $k$  (number on each curve in  $s^{-1}$ ) for typical values of  $k_D$  ( $10^{10} M^{-1} s^{-1}$ ),  $D$  ( $2 \times 10^{-5} cm^2 s^{-1}$ ), and  $R$  (3 Å). (b) Shift of the intersection potential  $E_1$  (see a) as a function of the follow-up reaction rate constant  $k$ .  $E_1 - E^\circ_{A/B}$  is a measure of the error for the determination of  $E^\circ_{A/B}$  made when the conversion of B into C within the solvent cage is ignored.

right, zero,  $\alpha F/RT$ , and  $F/RT$  slopes. They correspond to different controls of the forward reaction: diffusion control, activation control, and “counter-diffusion” control combined with control by the follow-up reaction taking place within the solvent cage. The first two asymptotes are the same whatever the value of  $k$ . The third is a function of  $k$ . Its location is represented in Figure 12b under the form of the variation of  $E_1 - E^\circ_{A/B}$  with  $k$ ,  $E_1$  being the intersection of the  $F/RT$  slope asymptote and the zero slope asymptote. It is seen in Figure 12b that the treatments on which eq 37 and 38 are based represent two limiting behaviors, one in which B does not diffuse and one in which it diffuses within the solvent cage according to Fick's law. The behavior in between would be a diffusion process occurring over too short a distance, as compared to molecular sizes, for Fick's law to be obeyed. On the other hand,  $E_1 - E^\circ_{A/B}$  is a measure of the error on the determination of  $E^\circ_{A/B}$  made when the conversion of B into C within the solvent cage is ignored.

Upon going to smaller driving forces, a fourth asymptote may be met corresponding to the passage from a stepwise to a concerted A-B-C process. Its slope is again  $\alpha F/RT$ , with however a value of  $\alpha$  corresponding to the concerted process rather than to the stepwise process. It is expected that the former will be significantly smaller than the latter since the electron transfer is exergonic ( $\alpha < 0.5$ ) in the concerted case and endergonic ( $\alpha > 0.5$ ) in the stepwise case. The passage from the stepwise to the concerted case will be more rapid the faster the follow-up reaction as represented in Figure 12. Taking  $6 \times 10^{12} M^{-1} s^{-1}$  as an estimate of

**TABLE III. Applications of the Redox Catalysis Method to the Investigation of the Kinetics of Electron-Transfer-Induced Reactions**

example	ref	mechanism
reductive cleavage of aryl halides	64, 73-75 <sup>a</sup>	ECE
reductive cleavage of aryl-substituted vinyl halides	76 <sup>b,c</sup>	$P + e^- \rightleftharpoons Q$
reductive cleavage of diphenyl sulfide	77 <sup>d</sup>	$Q + A \rightleftharpoons P + B$
reductive cleavage of sulfilimide	78 <sup>e</sup>	$B \rightarrow C$
reductive cleavage of aryl alkyl sulfides	78-81 <sup>d,e</sup>	$Q + C \rightarrow A + D$
reductive cleavage of tosyl ethers and amides	82 <sup>d</sup>	
reductively induced conformational changes of bianthrone	83, 84 <sup>d</sup>	
reductive elimination of halide ions in aliphatic vicinal dihalides yielding olefins in aryl-substituted vicinal dihalides	85, 86 <sup>c</sup>	dissociative EC or ECE $P + e^- \rightleftharpoons Q^{\cdot-}$
reductive cleavage of perfluoroalkyl bromides and iodides	87 <sup>c</sup> 88, 89 <sup>c</sup>	$Q^{\cdot-} + RX \rightarrow P + R^{\cdot} + X^-$ $R^{\cdot} \rightarrow \text{products or}$ $Q^{\cdot-} + R^{\cdot} \rightarrow P + R^{\cdot}$
reductive cleavage of CCl <sub>4</sub> , CBr <sub>4</sub> , CCl <sub>3</sub> Br	90-92 <sup>c</sup>	
reductive cleavage of aliphatic halides	72, 93-96 <sup>c</sup>	dissociative EC and addition on the mediator $P + e^- \rightleftharpoons Q^{\cdot-}$
reductive cleavage of benzyl halides	97	$Q^{\cdot-} + RX \rightarrow P + R^{\cdot} + X^-$ $Q^{\cdot-} + R^{\cdot} \rightarrow QR^{\cdot}$ or $Q^{\cdot-} + R^{\cdot} \rightarrow P + R^{\cdot}$
reductive cleavage of 9-chloro-9-mesitylfluorene and 9-chloro-9-( $\alpha$ -9-fluorenylidenebenzyl)fluorene	98 <sup>d</sup>	CE $P + e^- \rightleftharpoons Q^{\cdot-}$ $RX \rightleftharpoons R^+ + X^-$ $Q^{\cdot-} + R^+ \rightarrow P + R^{\cdot}$
reductive cleavage of 9-chloro-9-mesitylfluorene	99 <sup>d</sup>	autocatalysis $RX + 2e^- \rightarrow R^{\cdot} + X^-$ $RX + R^{\cdot} \rightarrow 2R^{\cdot} + X^-$ $R^{\cdot} + e^- \rightarrow R^{\cdot}$
electrochemically induced nucleophilic induced nucleophilic substitution of aryl halides	100, 101 <sup>d</sup>	electrocatalysis $P + e^- \rightleftharpoons Q^{\cdot-}$ $Q^{\cdot-} + ArX \rightarrow P + ArX^{\cdot-}$ $ArX^{\cdot-} \rightarrow Ar^{\cdot} + X^-$ $Ar^{\cdot} + Nu^- \rightarrow ArNu^{\cdot-}$ $P + ArNu^{\cdot-} \rightarrow ArNu$

<sup>a</sup>Determination of the cleavage rate constant up to  $5 \times 10^8 \text{ s}^{-1}$ . For faster cleavages, determination of the  $ArX/ArX^{\cdot-}$  standard potential and standard rate constant. <sup>b</sup>Whether the reaction follows an ECE-type mechanism or an EC dissociative mechanism is not ascertained for the moment. <sup>c</sup>Determination of the forward electron-transfer rate constant. <sup>d</sup>Determination of the rate constant of the chemical steps coupled with the electron-transfer step. <sup>e</sup>Determination of the standard potential and standard rate constant of the electron-transfer step.

the limit over which a concerted process prevails whatever the driving force, it can be seen (Figure 12) that the error on the determination of  $E_{A/B}^{\circ}$  made when the conversion of B into C within the solvent cage is ignored is small, at maximum on the order of 80 mV.<sup>65</sup>

In the preceding analysis, aimed at the determination of the standard potential and standard rate constant of the E step, it was implicitly assumed that the mediators in the series have approximately the same self-exchange intrinsic barrier so the Marcus activation-driving force relationship can be regarded as a true Brønsted plot.<sup>8</sup> If this restricting condition is removed, the analysis is still possible if the mediator self-exchange intrinsic barriers are known independently, using then the full expression of the Marcus cross-exchange equation.

In the case where a concerted EC mechanism is observed over the whole range of useable mediators, the sole kinetic information that can be extracted from the experimental data is the variation of the forward rate constant with the driving force represented by the standard potential of the mediator. In principle, a counter-diffusion line should appear at driving forces small enough for the standard potential of the mediator to be largely positive to the standard potential of the A/C couple (rather than that of the A/B couple). In the case where the C reaction involves the breaking of a bond, the rate constant would be very small in this

range of driving forces, hence difficult to be measured by the redox catalysis method, because these concerted electron transfer-bond breaking reactions possess a large intrinsic barrier. A recent modeling of such reactions indeed predicts a contribution of bond breaking to the intrinsic barrier equal to one-fourth of the bond dissociation energy.<sup>72</sup> There are however cases where the ABC reaction involves a less drastic internal reorganization, for example a conformational change, making less unlikely the occurrence of such a situation.

### C. Other Mechanisms. Experimental Examples

Mechanisms as simple as EC mechanisms are rarely found in current practice. In a large number of cases, the reaction starts in an EC fashion but further steps are involved. In such circumstances, the above analyses only require a slight modification to be used. In other cases, quite different reaction schemes are involved calling for a more profound adaptation of the preceding analyses although the basic principles remain the same. Table III summarizes the various examples of the use of the redox catalysis method that can be found in the literature.

Among the aryl halides, a particularly favorable situation is met as to the complete characterization of the kinetics in the reduction of 1-chloronaphthalene by the electrochemically generated anion radical of 4-meth-

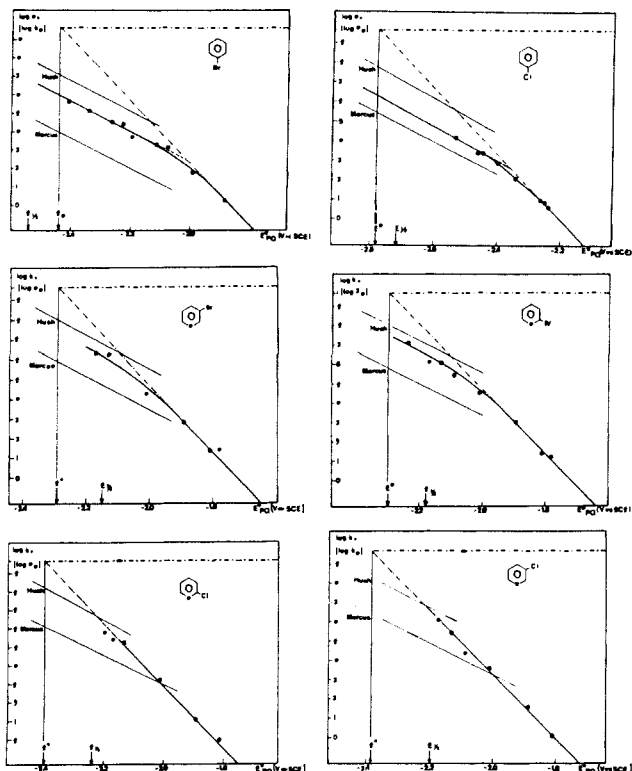


**Figure 13.** Forward electron-transfer rate constant  $k_+$  vs the standard potential  $E^\circ_{P/Q}$  of a series of aromatic anion radicals for fast cleaving aryl halide anion radicals (DMF, 20 °C).  $k_D$  is the bimolecular diffusion limit.

oxybenzophenone in DMSO.<sup>73</sup> The kinetic control passes from forward electron transfer to a mixed-control situation as the ArX concentration is increased. This indicates that the  $\text{ArX}^{\bullet-}$  radical is an intermediate since a concerted electron transfer–bond breaking pathway should only exhibit the first type of dependency toward the ArX concentration with no change upon raising [ArX]. The values of  $k_+$  and of  $k/k_-$  can thus be derived from the redox catalysis data. On the other hand, the cyclic voltammetry data indicate that, in the scan rate range 0.1–1000 V/s, the overall electrochemical reaction is kinetically controlled by the cleavage reaction. This also shows that the reaction goes through the  $\text{ArX}^{\bullet-}$  anion radical and, in addition, provides the value of  $E^\circ_{A/B} + (RT/F) \ln k$ . Since in the relationship  $(RT/F) \ln (k_+/k_-) = E^\circ_{A/B} - E^\circ_{P/Q}$  is known, one can derive all four unknowns,  $E^\circ_{A/B}$ ,  $k_+$ ,  $k_-$ , and  $k$ , from the combination of the above four relationships.  $k_-$  is thus found equal to the diffusion limit. In most cases such a complete determination of the kinetics cannot be achieved. However, as long as the redox catalysis data are such that the system passes from one of the two limiting controls to the mixed control, the value of  $k/k_-$  can be obtained. Since, in most cases,  $k_-$  can be proven to be at the diffusion limit,  $k$  ensues. Cleavage rate constants as high as  $5 \times 10^8 \text{ s}^{-1}$  have been determined in this way. The cleavage rate constants that are accessible by the method in the context of this ECE-type mechanism range from ca.  $10^5$  to  $10^9 \text{ s}^{-1}$ .

Continuing with aryl halide anion radicals, but with those that cleave faster than  $5 \times 10^8 \text{ s}^{-1}$ , Figure 13 shows typical examples of the determination of the standard potential and standard rate constant of the E step.

The reduction of triphenylmethyl phenyl sulfide<sup>81</sup> offers a quite interesting attempt to observe the passage

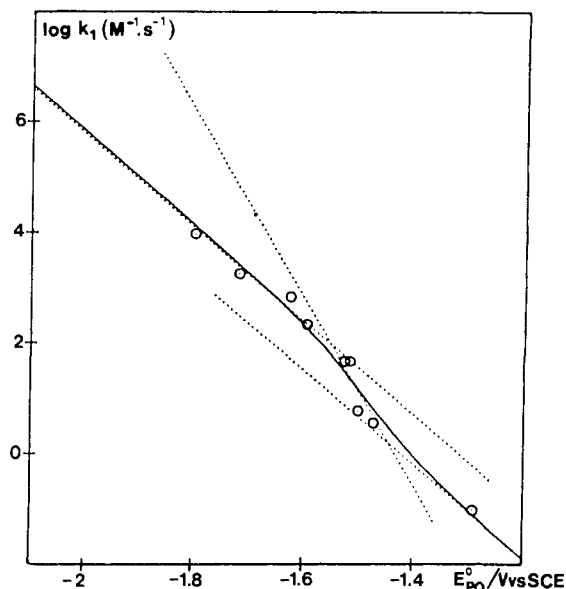


**Figure 14.** Reduction of  $\text{Ph}_3\text{CSPH}$  by electrochemically generated aromatic anion radicals (in DMF, at 25 °C). Variation of the rate-determining step rate constant  $k_+$  with the standard potential of the aromatic anion radical  $E^\circ_{P/Q}$ . From left to right: azobenzene, benzo[*c*]cinnoline, 4-(dimethylamino)azobenzene, terphenyl, naphthalene, phthalonitrile, perylene, fluoranthene, 9,10-diphenylanthracene. The dotted lines are the theoretical limiting behaviors corresponding to the concerted (right) and stepwise (left) pathways.

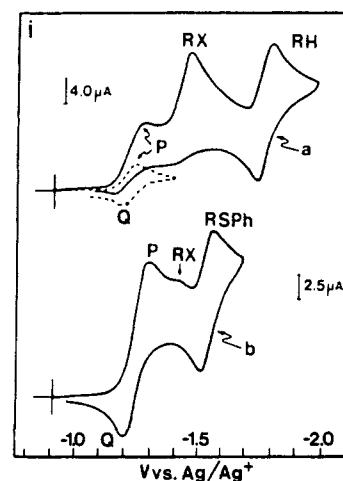


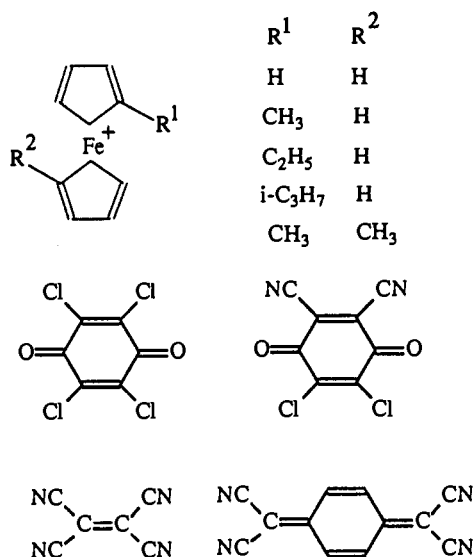
**Figure 15.** Indirect electrochemical induction of  $\text{S}_{\text{RN}}1$  reactions. Cyclic voltammetry of (a) 4-cyanopyridine (2.2 mM) in the absence (---) and presence of 8.9 mM 2-chlorobenzonitrile (—) and (b) 4-cyanopyridine (6.6 mM) in the presence of 8.9 mM 2-chlorobenzonitrile and 35 mM PhS<sup>-</sup>.

from a stepwise to a concerted pathway upon changing of the driving force. The reduction by aromatic anion radicals, having standard potentials more positive than the electrochemical reduction potential, is also charge-transfer-controlled. The variations of the rate constant with the driving force, as represented by the standard potential of the aromatic anion radical  $E^\circ_{P/Q}$  are shown in Figure 14. There is a small but distinct change of the curve on which the data points are located as the driving force of the reaction is decreased as predicted<sup>65</sup> for the passage from a stepwise to a concerted pathway.

In the case of aliphatic<sup>96,102</sup> and benzylic halides<sup>97</sup> as well as in that of trifluoromethyl bromide<sup>89</sup> and vicinal dibromides,<sup>85,86</sup> the data obtained with outer-sphere mediators, namely aromatic anion radicals, have been

extremely useful to know whether or not other electron donors (nucleophiles) function in the same way or rather in an inner-sphere fashion.

The diagnosis of the homogeneous CE mechanism is quite different from the preceding cases. The following mediators were used with the two triphenylmethyl-type chlorides, for which the  $R^+/R^-$  couple is reversible, and



also the  $R^+/R^-$  couple in the absence of chloride ions.<sup>99,103</sup> In most cases, the rate-determining step is the dissociation of the chloride as attested by the independence of the overall kinetics on both the standard potential and concentration of the mediator. Under these conditions, the follow-up electron-transfer step is at the diffusion limit as can be inferred from the quite large difference in standard potentials between the reductants and the  $R^+/R^-$  couple.<sup>99,103</sup> This is why the electron-transfer step is able to compete successfully with the coupling between  $R^+$  and  $Cl^-$ , a strongly downhill reaction. Mixed kinetic control by the cleavage reaction and the successive electron-transfer step was observed only with the most positive mediator, viz., 2,3-dicyano-5,6-dichloroquinone, for which the electron-transfer rate constant falls below the diffusion limit. The rate and equilibrium constants of the cleavage reaction were derived from the kinetic data. It is remarkable that the presence of a CE mechanism could not be detected in direct electrochemistry<sup>2</sup> of these two compounds whereas it could in the homogeneously mediated process.

The "redox catalysis of an electrocatalytic process" is also remarkably different in terms of diagnosis from all the preceding cases. One starts with the reversible wave of the mediator alone (see Figure 15). Upon addition of the aryl halide, it loses its reversibility and increases in height as a result of the redox catalysis of the reduction of the aryl halide as described earlier. Upon addition of the nucleophile, the P/Q wave decreases back and its reversibility is restored. The reduced form of the mediator Q reduces the aryl halide, which then cleaves off the halide ion, giving rise to the aryl radical that reacts with the nucleophile, thus producing the  $RNu^-$  anion radical. This is then reoxidized into the final substitution product by the oxidized form of the mediator. On the whole, the reaction consumes a vanishingly small amount of electrons ("electrocatalyzed process"), which explains why the

initial reversibility of the mediator wave is restored upon addition of the nucleophile.

#### IV. Concluding Remarks

Combining direct and indirect electrochemical techniques allows the determination of rate constants of coupled homogeneous chemical reactions in an extended domain, ranging from tens of seconds to nanoseconds in terms of intermediate lifetimes. En passant, precious information concerning the thermodynamics and kinetics of heterogeneous and homogeneous electron-transfer steps can be gathered. It is certainly a fascinating task to push these techniques further toward even higher rate constants. However, the evaluation and improvement of the precision in the already accessible range as well as its extension toward low values, situated in the gap between electrochemical techniques and classical chemical techniques, are also worthwhile.

#### References

- (1) Bard, A. J.; Faulkner, L. *Electrochemical methods*; Wiley: New York, 1980.
- (2) Andrieux, C. P.; Savéant, J.-M.; *Electrochemical Reactions. In Investigations of Rates and Mechanisms*; Bernasconi, C. F., Ed.; Wiley: New York, 1986; Vol. 6, 4/E, Part 2, pp 305-390.
- (3) Bridcka, R. *Collect. Czech. Chem. Commun.* 1947, 12, 522.
- (4) Bridcka, R.; Hanus, V.; Koutecky, J. *Progress in Polarography*; Zuman, P., Kolthoff, I. M., Eds.; Interscience: New York, 1962; pp 145-199.
- (5) Nürnberg, H. W.; Wolf, G. *J. Electroanal. Chem. Interfacial Electrochem.* 1969, 21, 99.
- (6) Savéant, J.-M. *Mechanisms and Reactivity in Organic Electrochemistry. In Advances in Electrochemistry*; The Robert A. Welsh Foundation: Houston, 1986; Chapter IV, pp 289-336.
- (7) Savéant, J.-M. *Bull. Soc. Chim. Fr.* 1988, 225.
- (8) Savéant, J.-M. *Adv. Phys. Org. Chem.*, in press.
- (9) Garreau, D.; Savéant, J.-M. *J. Electroanal. Chem. Interfacial Electrochem.* 1972, 35, 309.
- (10) Garreau, D.; Savéant, J.-M. *J. Electroanal. Chem. Interfacial Electrochem.* 1974, 50, 1.
- (11) Garreau, D.; Savéant, J.-M. *J. Electroanal. Chem. Interfacial Electrochem.* 1978, 86, 63.
- (12) Imbeaux, D.; Savéant, J.-M. *J. Electroanal. Chem. Interfacial Electrochem.* 1970, 28, 325.
- (13) Savéant, J.-M.; Tessier, D. *J. Electroanal. Chem. Interfacial Electrochem.* 1977, 77, 225.
- (14) Imbeaux, D.; Savéant, J.-M. *J. Electroanal. Chem. Interfacial Electrochem.* 1973, 44, 169.
- (15) Howell, J. O.; Wightman, R. M. *Anal. Chem.* 1984, 56, 524.
- (16) Robinson, R. S.; McCreery, R. L. *Anal. Chem.* 1981, 53, 997.
- (17) Robinson, R. S.; McCurdy, C. W.; McCreery, R. L. *Anal. Chem.* 1982, 54, 2356.
- (18) Wightman, R. M.; Wipf, D. O. In *Electroanalytical Chemistry*; Bard, A. J., Ed.; Marcel Dekker: New York, 1989; Vol. 15, pp 267-353.
- (19) Fleischmann, M.; Pons, S. In *Ultramicroelectrodes*; Fleischmann, M., Pons, S., Shmidt, P. P., Eds.; Datatech: Morganton, NC, 1987; pp 1-63.
- (20) Wipf, D. O.; Michael, A. C.; Wightman, R. M. *J. Electroanal. Chem. Interfacial Electrochem.* 1989, 269, 15.
- (21) Howell, J. O.; Kuhr, W. G.; Ensmann, R. E.; Wightman, R. M. *J. Electroanal. Chem. Interfacial Electrochem.* 1986, 209, 77.
- (22) Wipf, D. O.; Kristensen, E. W.; Deakin, M. R.; Wightman, R. M. *Anal. Chem.* 1988, 60, 306.
- (23) Wipf, D. O.; Wightman, R. M. *Anal. Chem.* 1988, 60, 2460.
- (24) Andrieux, C. P.; Garreau, D.; Hapiot, P.; Pinson, J.; Savéant, J.-M. *J. Electroanal. Chem. Interfacial Electrochem.* 1988, 243, 321.
- (25) Andrieux, C. P.; Garreau, D.; Hapiot, P.; Savéant, J.-M. *J. Electroanal. Chem. Interfacial Electrochem.* 1988, 248, 447.
- (26) Garreau, D.; Hapiot, P.; Savéant, J.-M. *J. Electroanal. Chem. Interfacial Electrochem.* 1989, 272, 1.
- (27) Baranski, A. S.; Lu, W. *J. Electroanal. Chem. Interfacial Electrochem.* 1989, 260, 1.
- (28) Delahay, P. *New Instrumental Methods in Electrochemistry*; Interscience: New York, 1954.
- (29) Bowyer, W. J.; Engleman, E. E.; Evans, D. H. *J. Electroanal. Chem. Interfacial Electrochem.* 1989, 262, 67.

- (30) Amatore, C.; Lefrou, C.; Pflüger, F. *J. Electroanal. Chem. Interfacial Electrochem.* **1989**, *270*, 43.
- (31) Garreau, D.; Hapiot, P.; Savéant, J.-M. *J. Electroanal. Chem. Interfacial Electrochem.* **1990**, *289*, 73.
- (32) Andrieux, C. P.; Hapiot, P.; Savéant, J.-M. *J. Phys. Chem.* **1988**, *92*, 5992.
- (33) Montenegro, M. I.; Pletcher, D. *J. Electroanal. Chem. Interfacial Electrochem.* **1986**, *200*, 371.
- (34) Kojima, H.; Bard, A. J. *Am. Chem. Soc.* **1975**, *97*, 6317.
- (35) Howell, J. O.; Goncalves, J.; Amatore, C.; Klasinc, L.; Kochi, J.; Wightman, R. M. *J. Am. Chem. Soc.* **1984**, *106*, 3968.
- (36) Howell, J. O.; Wightman, R. M. *J. Phys. Chem.* **1984**, *88*, 5992.
- (37) Anxolabéhère, E.; Hapiot, P.; Savéant, J.-M. *J. Electroanal. Chem. Interfacial Electrochem.* **1990**, *282*, 275.
- (38) Wipf, D. O.; Wehmeyer, K. R.; Wightman, R. M. *J. Org. Chem.* **1986**, *51*, 4760.
- (39) Wehmeyer, K. R.; Wightman, R. M. *Anal. Chem.* **1985**, *57*, 1989.
- (40) Andrieux, C. P.; Audebert, P.; Hapiot, P.; Savéant, J.-M. *J. Am. Chem. Soc.* **1990**, *112*, 2439.
- (41) Amatore, C.; Jutand, A.; Pflüger, F. *J. Electroanal. Chem. Interfacial Electrochem.* **1987**, *218*, 361.
- (42) Fitch, A.; Evans, D. H. *J. Electroanal. Chem. Interfacial Electrochem.* **1986**, *202*, 83.
- (43) Andrieux, C. P.; Hapiot, P.; Savéant, J.-M. *J. Phys. Chem.* **1988**, *92*, 5987.
- (44) Wipf, D. O.; Wightman, R. M. *J. Phys. Chem.* **1989**, *93*, 4286.
- (45) Hapiot, P.; Moiroux, J.; Savéant, J.-M. *J. Am. Chem. Soc.* **1990**, *112*, 1337.
- (46) Savéant, J.-M. *Acc. Chem. Res.* **1980**, *13*, 323.
- (47) Bunnett, J. F. *Acc. Chem. Res.* **1978**, *11*, 413.
- (48) Amatore, C.; Chaussard, J.; Pinson, J.; Savéant, J.-M.; Thiebault, A. *J. Am. Chem. Soc.* **1979**, *101*, 6012.
- (49) M'Halla, F.; Pinson, J.; Savéant, J.-M. *J. Am. Chem. Soc.* **1980**, *102*, 4120.
- (50) Amatore, C.; Savéant, J.-M. *J. Electroanal. Chem. Interfacial Electrochem.* **1981**, *123*, 189.
- (51) Amatore, C.; Savéant, J.-M. *J. Electroanal. Chem. Interfacial Electrochem.* **1981**, *123*, 203.
- (52) Amatore, C.; M'Halla, F.; Savéant, J.-M. *J. Electroanal. Chem. Interfacial Electrochem.* **1981**, *123*, 219.
- (53) Amatore, C.; Pinson, J.; Savéant, J.-M.; Thiebault, A. *J. Electroanal. Chem. Interfacial Electrochem.* **1981**, *123*, 231.
- (54) Amatore, C.; Savéant, J.-M. *J. Electroanal. Chem. Interfacial Electrochem.* **1981**, *125*, 1.
- (55) Amatore, C.; Savéant, J.-M. *J. Electroanal. Chem. Interfacial Electrochem.* **1982**, *126*, 1.
- (56) Amatore, C.; Guidelli, R.; Moncelli, M. R.; Savéant, J.-M. *J. Electroanal. Chem. Interfacial Electrochem.* **1983**, *148*, 25.
- (57) Savéant, J.-M. *J. Electroanal. Chem. Interfacial Electrochem.* **1987**, *236*, 31.
- (58) Wendt, H.; Plzak, V. *J. Electroanal. Chem. Interfacial Electrochem.* **1983**, *154*, 13.
- (59) Plzak, V.; Wendt, H. *J. Electroanal. Chem. Interfacial Electrochem.* **1983**, *154*, 129.
- (60) Plzak, V.; Wendt, H. *J. Electroanal. Chem. Interfacial Electrochem.* **1984**, *180*, 185.
- (61) Amatore, C.; Savéant, J.-M. *J. Am. Chem. Soc.* **1981**, *103*, 5021.
- (62) Andrieux, C. P.; Dumas-Bouchiat, J.-M.; Savéant, J.-M. *J. Electroanal. Chem. Interfacial Electrochem.* **1980**, *113*, 1.
- (63) Andrieux, C. P.; Dumas-Bouchiat, J.-M.; Savéant, J.-M. *J. Electroanal. Chem. Interfacial Electrochem.* **1980**, *113*, 19.
- (64) Andrieux, C. P.; Blocman, C.; Dumas-Bouchiat, J.-M.; Savéant, J.-M. *J. Am. Chem. Soc.* **1979**, *101*, 3431.
- (65) Andrieux, C. P.; Savéant, J.-M. *J. Electroanal. Chem. Interfacial Electrochem.* **1986**, *205*, 43.
- (66) Marcus, R. A.; Sutin, N. *Biophys. Biochim. Acta* **1985**, *811*, 265.
- (67) Smoluchovski, M. *Phys. Z.* **1916**, *17*, 557.
- (68) Smoluchovski, M. *Phys. Z.* **1916**, *17*, 585.
- (69) Smoluchovski, M. *Z. Phys. Chem., Stoechiom. Verwandtschaftsl.* **1917**, *92*, 129.
- (70) Debye, P. *Trans. Electrochem. Soc.* **1942**, *82*, 265.
- (71) Grimshaw, J.; Thompson, N. *J. Electroanal. Chem. Interfacial Electrochem.* **1986**, *205*, 35.
- (72) Savéant, J.-M. *J. Am. Chem. Soc.* **1987**, *109*, 6788.
- (73) Andrieux, C. P.; Blocman, C.; Dumas-Bouchiat, J.-M.; M'Halla, F.; Savéant, J.-M. *J. Am. Chem. Soc.* **1980**, *102*, 3806.
- (74) Andrieux, C. P.; Savéant, J.-M.; Zann, O. *Nouv. J. Chim.* **1984**, *8*, 107.
- (75) Arena, J. V.; Rusling, J. F. *J. Phys. Chem.* **1987**, *91*, 3368.
- (76) Gatti, N.; Jugelt, W.; Lund, H. *Acta Chem. Scand.* **1987**, *B41*, 646.
- (77) Griggio, L. *J. Electroanal. Chem. Interfacial Electrochem.* **1982**, *140*, 315.
- (78) Griggio, L.; Severin, M. G. *J. Electroanal. Chem.* **1987**, *123*, 185.
- (79) Capobianco, C.; Farnia, G.; Severin, M. G.; Vianello, E. *J. Electroanal. Chem. Interfacial Electrochem.* **1984**, *165*, 251.
- (80) Severin, M. G.; Arevalo, M. C.; Farnia, G.; Vianello, E. *J. Phys. Chem.* **1987**, *91*, 466.
- (81) Severin, M. G.; Farnia, G.; Vianello, E.; Arevalo, M. C. *J. Electroanal. Chem. Interfacial Electrochem.* **1988**, *251*, 369.
- (82) Maia, H. L. S.; Meideiros, M. S.; Montenegro, M. I.; Court, D.; Pletcher, D. *J. Electroanal. Chem. Interfacial Electrochem.* **1984**, *164*, 347.
- (83) Evans, D. H.; Naxian, X. *J. Electroanal. Chem. Interfacial Electrochem.* **1982**, *133*, 367.
- (84) Evans, D. H.; Naxian, X. *J. Am. Chem. Soc.* **1983**, *105*, 355.
- (85) Lexa, D.; Savéant, J.-M.; Su, K. B.; Wang, D. L. *J. Am. Chem. Soc.* **1987**, *109*, 646.
- (86) Lexa, D.; Savéant, J.-M.; Schäfer, H.; Su, K. B.; Vering, B.; Wang, D. L. *J. Am. Chem. Soc.*, in press.
- (87) Lund, T.; Pedersen, S. U.; Lund, H.; Cheung, K. W.; Utley, J. P. *Acta Chem. Scand.* **1987**, *B41*, 285.
- (88) Andrieux, C. P.; Gelis, L.; Medebielle, M.; Pinson, J.; Savéant, J.-M. *J. Am. Chem. Soc.* **1990**, *112*, 3509.
- (89) Andrieux, C. P.; Gelis, L.; Savéant, J.-M. *J. Am. Chem. Soc.* **1990**, *112*, 786.
- (90) Ebersson, L.; Ekström, M. *Acta Chem. Scand.* **1988**, *B42*, 101.
- (91) Ebersson, L.; Ekström, M. *Acta Chem. Scand.* **1988**, *B42*, 113.
- (92) Ebersson, L.; Ekström, M.; Lund, T.; Lund, H. *Acta Chem. Scand.* **1989**, *43*, 101.
- (93) Lexa, D.; Mispelter, J.; Savéant, J.-M. *J. Am. Chem. Soc.* **1981**, *103*, 6806.
- (94) Andrieux, C. P.; Gallardo, I.; Savéant, J.-M.; Su, K. B. *J. Am. Chem. Soc.* **1986**, *108*, 638.
- (95) Andrieux, C. P.; Savéant, J.-M.; Su, K. B. *J. Phys. Chem.* **1986**, *90*, 3815.
- (96) Lund, T.; Lund, H. *Acta Chem. Scand.* **1986**, *B40*, 470.
- (97) Lund, T.; Lund, H. *Acta Chem. Scand.* **1987**, *B41*, 93.
- (98) Andrieux, C. P.; Merz, A.; Savéant, J.-M.; Tomahogh, R. *J. Am. Chem. Soc.* **1984**, *106*, 1957.
- (99) Andrieux, C. P.; Merz, A.; Savéant, J.-M. *J. Am. Chem. Soc.* **1985**, *107*, 6097.
- (100) Amatore, C.; Oturan, M. A.; Pinson, J.; Savéant, J.-M.; Thiebault, A. *J. Am. Chem. Soc.* **1984**, *106*, 6318.
- (101) Amatore, C.; Oturan, M. A.; Pinson, J.; Savéant, J.-M.; Thiebault, A. *J. Am. Chem. Soc.* **1985**, *107*, 3451.
- (102) Lexa, D.; Savéant, J.-M.; Su, K. B.; Wang, D. L. *J. Am. Chem. Soc.* **1988**, *110*, 7617.
- (103) Merz, A.; Tomahogh, R. *Angew. Chem., Int. Ed. Engl.* **1979**, *18*, 938.